SSC-358

STRUCTURAL BEHAVIOR AFTER FATIGUE

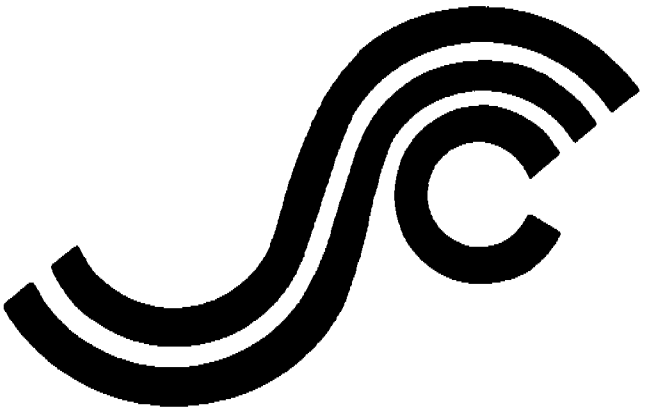

SHIP STRUCTURE COMMITTEE

1990

SHIP STRUCTURE COMMITTEE

The SHIP STRUCTURE COMMITTEE is constituted to prosecute a research program to improve the hull structures of ships and other marine structures by an extension of knowledge pertaining to design, materials, and methods of construction.

RADM J. D. Sipes, USCG, (Chairman)
Chief, Office of Marine Safety, Security and Environmental Protection
U. S. Coast Guard

Mr. Alexander Malakhoff
Director, Structural Integrity Subgroup (SEA 55Y)
Naval Sea Systems Command

Dr. Donald Liu
Senior Vice President
American Bureau of Shipping

Mr. H. T. Haller
Associate Administrator for Ship-building and Ship Operations
Maritime Administration

Mr. Thomas W. Allen
Engineering Officer (N7)
Military Sealift Command

CDR Michael K. Parmelee, USCG,
Secretary, Ship Structure Committee
U. S. Coast Guard

CONTRACTING OFFICER TECHNICAL REPRESENTATIVES

Mr. William J. Siekierka
SEA 55Y3
Naval Sea Systems Command

Mr. Greg D. Woods
SEA 55Y3
Naval Sea Systems Command

SHIP STRUCTURE SUBCOMMITTEE

The SHIP STRUCTURE SUBCOMMITTEE acts for the Ship Structure Committee on technical matters by providing technical coordination for determinating the goals and objectives of the program and by evaluating and interpreting the results in terms of structural design, construction, and operation.

AMERICAN BUREAU OF SHIPPING

Mr. Stephen G. Arntson (Chairman)
Mr. John F. Conlon
Mr. William Hanzalek
Mr. Philip G. Rynn

MILITARY SEALIFT COMMAND

Mr. Albert J. Attermeyer
Mr. Michael W. Touma
Mr. Jeffery E. Beach

MARITIME ADMINISTRATION

Mr. Frederick Seibold
Mr. Norman O. Hammer
Mr. Chao H. Lin
Dr. Walter M. Maclean

NAVAL SEA SYSTEMS COMMAND

Mr. Robert A. Sielski
Mr. Charles L. Null
Mr. W. Thomas Packard
Mr. Allen H. Engle

U. S. COAST GUARD

CAPT T. E. Thompson
CAPT Donald S. Jensen
CDR Mark E. Noll

SHIP STRUCTURE SUBCOMMITTEE LIAISON MEMBERS

U. S. COAST GUARD ACADEMY

LT Bruce Mustain

U. S. MERCHANT MARINE ACADEMY

Dr. C. B. Kim

U. S. NAVAL ACADEMY

Dr. Ramswar Bhattacharyya

STATE UNIVERSITY OF NEW YORK MARITIME COLLEGE

Dr. W. R. Porter

WELDING RESEARCH COUNCIL

Dr. Martin Prager

NATIONAL ACADEMY OF SCIENCES - MARINE BOARD

Mr. Alexander B. Stavovy

NATIONAL ACADEMY OF SCIENCES - COMMITTEE ON MARINE STRUCTURES

Mr. Stanley G. Stiansen

SOCIETY OF NAVAL ARCHITECTS AND MARINE ENGINEERS - HYDRODYNAMICS COMMITTEE

Dr. William Sandberg

AMERICAN IRON AND STEEL INSTITUTE

Mr. Alexander D. Wilson

Member Agencies:

United States Coast Guard
Naval Sea Systems Command
Maritime Administration
American Bureau of Shipping
Military Sealift Command

Ship Structure Committee

An Interagency Advisory Committee
Dedicated to the Improvement of Marine Structures

Address Correspondence to:

Secretary, Ship Structure Committee
U.S. Coast Guard (G-MTH)
2100 Second Street S.W.
Washington, D.C. 20593-0001
PH: (202) 267-0003
FAX: (202) 267-0025

SSC-358
SR-1301

December 3, 1990

STRUCTURAL BEHAVIOR AFTER FATIGUE

Cyclic loading can lead to changes in the mechanical properties of materials. This project examined the extent that cyclic loading influences the fatigue crack propagation and fracture toughness behavior of steels. The findings and an evaluation of the causes for the change in material properties are included in this report.

J. D. SIPES
Rear Admiral, U.S. Coast Guard
Chairman, Ship Structure Committee

Technical Report Documentation Page

1. Report No.	2 Government Accession No.	3. Recipient's Catalog No.
SSC-358	-	-

4. Title and Subtitle	5. Report Date
Influence of Prior Damage by Cyclic Loading Below the Yield Strength on Ship Steels in Marine Environments	August, 1987
	6. Performing Organization Code: SR-1301
7. Author(s): Brian N. Leis	8. Performing Organization Report No.: -
9. Performing Organization Name and Address: Battelle, Columbus Division, 505 King Avenue, Columbus, Ohio 43201-2693	10. Work Unit No (TRAIS): -
	11. Contract or Grant No.: DTCG23-84-C-20083
12. Sponsoring Agency Name and Address: Commandant, U. S. Coast Guard, Washington, D.C. 20593	13. Type of Report and Period Covered: Final
	14 Sponsoring Agency Code: G-M

15 Supplementary Notes

Work sponsored by the Ship Structure Committee and its member agencies.

16 Abstract

This study examines the extent to which prior cyclic history, which causes a change in mechanical properties through cyclic softening, influences the fatigue crack propagation (FCP) and fracture toughness behavior of ABS EH36 and HY80. The effect of predamage was determined empirically by comparing fracture toughness and FCP behavior developed for virgin materials with that found for predamaged materials. The scope of the study included testing under ambient conditions as well as in seawater at frequencies as low as 0.2 Hz.

The data developed have been analyzed to assess whether apparent predamage effects are due to inherent changes in the material or are a consequence of the effects of cyclic softening on the validity and uniqueness of the test methods as applied in past studies. The main conclusion of the study was that apparent predamage effects are due to the influence of cyclic softening on the test methods and related data interpretation. When J_{Ic} is used as the basis to assess fracture toughness, the difference between virgin and predamaged toughnesses was negligible. Likewise, fatigue crack growth rates were similiar. for virgin and predamaged materials provided that crack closure was accounted for by using the range of the effective stress intensity factor to correlate growth rates.

17 Key Words	18. Distribution Statement
fracture toughness, fatigue crack propagation, ABS EH36, HY80, seawater, crack-closure, cyclic predamage	DOCUMENT IS AVAILABLE TO THE PUBLIC THROUGH THE NATIONAL TECHNICAL INFORMATION SERVICE, SPRINGFIELD VIRGINIA 22161

19 Security Classif (of this report)	20 Security Classif (of this page)	21. No of Pages	22. Price
UNCLASSIFIED	UNCLASSIFIED	84	

Form DOT F1700.7 (8-72) Reproduction of completed page authorized

METRIC CONVERSION FACTORS

Approximate Conversions to Metric Measures

Symbol	When You Know	Multiply by	To Find	Symbol
	LENGTH			
in	inches	*2.5	centimeters	cm
ft	feet	30	centimeters	cm
yd	yards	0.9	meters	m
mi	miles	1.6	kilometers	km
	AREA			
in^2	square inches	6.5	square centimeters	cm^2
ft^2	square feet	0.09	square meters	m^2
yd^2	square yards	0.8	square meters	m^2
mi^2	square miles	2.6	square kilometers	km^2
	acres	0.4	hectares	ha
	MASS (weight)			
oz	ounces	28	grams	g
lb	pounds	0.45	kilograms	kg
	short tons (2000 lb)	0.9	tonnes	t
	VOLUME			
tsp	teaspoons	5	milliliters	ml
Tbsp	tablespoons	15	milliliters	ml
fl oz	fluid ounces	30	milliliters	ml
c	cups	0.24	liters	l
pt	pints	0.47	liters	l
qt	quarts	0.95	liters	l
gal	gallons	3.8	liters	l
ft^3	cubic feet	0.03	cubic meters	m^3
yd^3	cubic yards	0.76	cubic meters	m^3
	TEMPERATURE (exact)			
°F	Fahrenheit temperature	5/9 (after subtracting 32)	Celsius temperature	°C

*1 in = 2.54 (exactly). For other exact conversions and more detailed tables, see NBS Misc. Publ. 286, Units of Weights and Measures, Price $2.25, SD Catalog No. C13.10:286.

Approximate Conversions from Metric Measures

Symbol	When You Know	Multiply by	To Find	Symbol
	LENGTH			
mm	millimeters	0.04	inches	in
cm	centimeters	0.4	inches	in
m	meters	3.3	feet	ft
m	meters	1.1	yards	yd
km	kilometers	0.6	miles	mi
	AREA			
cm^2	square centimeters	0.16	square inches	in^2
m^2	square meters	1.2	square yards	yd^2
km^2	square kilometers	0.4	square miles	mi^2
ha	hectares (10,000 m^2)	2.5	acres	
	MASS (weight)			
g	grams	0.035	ounces	oz
kg	kilograms	2.2	pounds	lb
t	tonnes (1000 kg)	1.1	short tons	
	VOLUME			
ml	milliliters	0.03	fluid ounces	fl oz
l	liters	2.1	pints	pt
l	liters	1.06	quarts	qt
l	liters	0.26	gallons	gal
m^3	cubic meters	35	cubic feet	ft^3
m^3	cubic meters	1.3	cubic yards	yd^3
	TEMPERATURE (exact)			
°C	Celsius temperature	9/5 (then add 32)	Fahrenheit temperature	°F

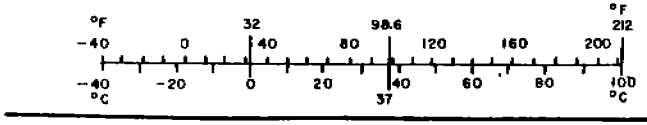

TABLE OF CONTENTS

LIST OF TABLES

LIST OF FIGURES

LIST OF FIGURES
(Continued)

INFLUENCE OF PRIOR DAMAGE BY CYCLIC LOADING BELOW THE YIELD STRENGTH ON SHIP STEELS IN MARINE ENVIRONMENTS

by

Brian N. Leis

1. INTRODUCTION

Data published in the 1970's imply that prior cyclic mechanical history influences the fracture properties of metals, e.g.,[1-6]. In all cases, an effect was found as a result of cycling prior to the formation of related microcracks. The effect has been manifested in regard to fracture toughness in two ways. First, data for a rotor steel[1], a pressure vessel steel[2] and an aluminum alloy[5] all show fatigue crack growth continues stably at values of K_{max} greater than K_{Ic}. In some cases, stable fatigue growth occurred until K_{max} was much greater than K_{Ic}. Second, consistent with this observation, fatigue-crack-tests precracked under load control at various load levels often develop values of K_Q that exceed K_{Ic}[1,4]. However, other observations which fail to indicate an effect of prior mechanical history cannot be so simply explained--as in some aluminum alloys[5], a high strength steel[7], and a rail steel[8]--or those which show a decreased toughness[6].

From a linear-elastic-fracture-mechanics (LEFM) fitness-for-service perspective, increased apparent toughness due to stress state effects has long been known[9]. It has been accounted for in design and analysis by the use of the lower-bound plane-strain toughness. The need for such a lower-bound toughness to avoid fracture problems motivated the fracture community in the early 1960's to develop ASTM E399[10]--a test method designed to produce a plane strain, hopefully lower-bound toughness value.

The E399 toughness standard will produce valid measures of K_{Ic} only so long as the requirements of the standard are satisfied to ensure that a plane-strain condition develops. The standard for developing fatigue crack-

growth-rate data (ASTM E647)[11] is, in many ways, similar to E399 except that it relaxes the plane strain thickness requirement of E399 to admit testing of section thicknesses similar to service conditions. Accordingly, the earlier statement that, in fatigue crack growth studies, values of K_Q in excess of K_{Ic} are observed is not surprising when the thickness requirement is relaxed. From a fitness-for-service perspective, results developed using E647 combined with E399 will provide a viable basis for design or analysis provided that they reflect service conditions (thickness, microstructure, etc.) or represent lower bound lives or critical crack sizes. If, however, prior damage* in some way violates conditions to ensure lower bound critical crack sizes or lives as compared to virgin material results which satisfied those conditions, these standards will fail to meet their intended goal. Clearly, data which show a decrease in toughness, such as discussed above, provide cause for concern since use of the standards to generate design data apparently no longer guarantees lower-bound lives.

The question of why prior cyclic history causes an apparent decrease in toughness must be asked and answered on an application-specific basis to ascertain if predamage causes an inherent reduction in material properties, or something associated with the predamage violates conditions to ensure lower-bound results that are otherwise satisfied by the virgin material. Moreover, if prior history can reduce toughness, there may be cause for concern in regard to predamage reducing properties for other mechanisms of growth such as fatigue.

This study examines the effects of cyclic predamage on toughness and fatigue-crack-growth rate. Specifically, this study explores the extent to which prior cyclic history, which causes some form of damage prior to microcracking, influences the fatigue-crack-propagation (FCP) and toughness behavior of ABS EH36 and HY80. Included in the study was (1) the definition and development of measurable damage, and (2) data generation with and without

---

* The term "damage" is used herein to represent the effects of cyclic mechanical loading, hereafter written as "cyclic loading" for the sake of brevity. Use of the term "damage" follows from the use of this term in the literature to represent cumulative changes in a material's state that leads to, and for some authors also includes microcrack initiation and limited microcrack growth. Use of the term "damage is not restricted in the literature to cyclic loading.

damage, in air as well as a marine environment, under loading conditions approaching service conditions. Following a section outlining the objective and scope, sections detailing the experimental method, results, and analyses are presented leading to a summary and the conclusions.

2. EXECUTIVE SUMMARY

This study examines the extent to which prior cyclic history, which causes a change in mechanical properties through cyclic softening, influences the fatigue crack propagation (FCP) and fracture toughness behavior of ABS EH36 and HY80. Cyclic loading that leads to changes in mechanical properties and eventual fatigue crack initiation and propagation is termed "damage" in the fatigue literature during the stage of life prior to microcrack (visible crack) formation. This study focuses on the effects of cyclic mechanical loading prior to the formation of macrocracks and, as such, the effects of the cycling are termed "damage". Because this damage is imposed prior to subsequent testing to develop data characterizing FCP and fracture toughness, this cycling is termed "predamage". The predamage was imposed by displacement controlled cycling of large panels from which blanks for FCP and fracture toughness were cut. Fatigue crack propagation was studied using a multicracked-tension-loaded panel, with the testing done within the spirit of ASTM E647. Fracture toughness was characterized using the J-R curve developed with compact tension specimens tested within the spirit of ASTM E813.

The effect of predamage was determined empirically by comparing fracture toughness and FCP behavior developed for virgin materials with that found for predamaged materials. The scope of the study included testing under ambient conditions as well as in seawater at frequencies as low as 0.2 Hz.

The data developed have been analyzed to assess whether apparent predamage effects are due to inherent changes in the material or are a consequence of the effects of cyclic softening on the validity and uniqueness of the test methods as applied in past studies. The main conclusion of the study was that apparent predamage effects are due to the influence of cyclic softening on the test methods and related data interpretation. When J_{Ic} is used as the basis to assess fracture toughness, the difference between virgin and predamaged toughnesses was negligible. Likewise, fatigue crack growth

rates were similar for virgin and predamaged materials provided that crack closure was accounted for by using the range of the effective stress intensity factor to correlate growth rates.

3. OBJECTIVE, SCOPE AND APPROACH

The objective of this study was to determine phenomenologically whether or not damage that influences fatigue crack growth and fracture toughness properties is produced by cyclic loading below the yield stress, before the appearance of cracks. A related objective was to isolate whether apparent predamage effects are real or are due to differences in test conditions caused by the predamage or other aspects of the test.

Meeting the objective requires first determining how to impose measurable predamage and then comparing the fatigue and fracture properties of undamaged--or virgin material--to those for damaged material. To maximize the effect of damage, the maximum damage state admitted by the objective should be explored. That is, cyclic damage below the yield stress should be imposed in some directly measurable way, subject to the constraint that the damage does not cause cracking at some high level of magnification.

The scope of this study was limited to ABS EH36 ship plate and HY80 ship plate. Data were developed to represent undamaged (virgin) material under ambient air conditions as well as seawater conditions. The possible effect of predamage on toughness and crack growth was determined by contrasting data for virgin steel with data developed for damaged/ambient and damaged/seawater conditions. Thus the approach was to empirically assess the effect of damage for these marine-specific situations.

4. EXPERIMENTAL DETAILS

4.a. Cyclic (Fatigue) Predamage and the Experimental Program

4.a.1. Guidance from the Literature

Perhaps the most extensive recent work on this subject has been done by Troshchenko and his colleagues (see [12,13] for reviews). Troshchenko et al have studied a broad range of steels and have concentrated their efforts at low to cryogenic temperatures. Their results indicate that in some cases steels which cyclically soften at low strains and harden at high strains show a reduced fracture toughness when the material element at the crack tip has been subjected to fatigue cycling. Significantly, strain levels that precondition near-crack-tip material elements are large and probably tend to harden that material. Troshchenko et al have also shown growth rates increase in such cases, at near unstable growth rate conditions. In some cases, the data developed by Troshchenko fail to show any change in toughness as a result of prior cycling.

Dowling[14] performed tests similar to those of Troshchenko on a steam turbine disk steel, ASTM A470, which cyclically softens. Dowling observed that toughness was controlled by the limit load, and found the toughness with prior cycling was well in excess of that of virgin material tested in accordance with ASTM 399**. Dowling maintains[15] that material which cyclically softens will show increased toughness. This view is shared provided that the loading rate and the environment are further restricted such that limit load conditions can indeed be developed, and that the increased toughness is demonstrated to be independent of test conditions. In such cases, tests like J_{Ic} are required for comparison of predamaged material data with the reference virgin material data to minimize confusion related to cyclic transient stress-strain response. In contrast to Dowling's results for

---

** Comparison of a limit load (plane stress) result with a plane strain E399 valid result is puzzling. Increased toughness is possibly a result of comparing plane stress and plane strain results. As such, "the material toughness" may not have changed, but the basis for comparison may have, as a result of prior cycling.

steels, Dowling discussed unpublished results of J. Begley for an aluminum alloy which cyclically hardened. Dowling noted that for the aluminum alloy the cyclic and virgin material toughnesses were coincident. While Dowling's view[15] is that this coincidence may be traced to the fact that the aluminum alloy hardened, this coincidence may also be traced to the fact that the conditions of ASTM E399 were still satisfied in the predamaged material.

Landes and Leax[16] studied an AISI 4340 steel, another steel which cyclically softens. Ductile toughness was studied using J-R curve techniques, with consideration given to the effects of 4 types of prior (predamage) histories. In cases where prior history was imposed in cracked bodies, the above discussion leads to interpretation of the test condition and results as ductility exhaustion during the history, leading to a decrease in toughness. Conversely, histories that produced softening and increased ductility would and indeed did produce slightly increased toughness as compared to virgin material.

Clarke[17] has explored the influence of prior mechanical history on the threshold for stress corrosion cracking in an H_2S environment. His conclusion was that predamage causing mechanical strengthening decreased the threshold in the same manner that heat treatment served to increase strength.

Gerberich and Moody[18] reviewed threshold trends for steels in ambient environments. They concluded that threshold increased with grain size for low strength steels but decreased with grain size for high strength steels. Grain size and strength are related in fatigue, and fatigue cycling often causes changes in grain size (e.g., see [19]). Thus, on the basis of these observations, the threshold may be expected to change as a function of hardening or softening due to fatigue cycling.

It should be emphasized that crack closure may be a major consideration in understanding the threshold behavior of long and short cracks. It may be a factor in explaining Gerberich's data. Moreover, differences in closure are expected as a function of material strength if closure is caused by residual plasticity in the wake of the crack. This follows from the fact that the plastic zone is roughly inversely proportional to the square of the yield stress. Softening by nearly a factor of 2--not unusual at small strains for ABS EH36[20] or HY80[21]--thus would cause about a fourfold increase in plastic zone size. For the same range of crack-tip-opening displacement (CTOD) (ΔK^2 in LEFM), this fourfold increase results in an increased wake due to the

increased flow and increased closure. In turn, for the same ΔCTOD, this softening is anticipated to cause a decrease in ΔK_{eff} and an increased threshold based on ΔK. But, this apparent increase in threshold is a result of a change in closure due to softening. It does not indicate an inherent increased resistance to cracking, since the apparent increase depends on how the data are analyzed.

The point to be made is that what appears to be an increased resistance to cracking may be artificial.*** When data are plotted in terms of ΔK_{eff}, this apparent increase in threshold due to closure will not be observed. Consequently, care must be taken in comparing crack growth rates to isolate the influence of prior cycles that cause softening. It follows that comparisons of virgin and predamaged material data should be based on ΔK_{eff}, both near the threshold and at finite rates to avoid closure-induced increases in threshold that depend on the ΔK history and the specimen (component) size and geometry.

A solid basis for comparison is also required in the study of toughness for precycled and virgin material. In many of the above cited studies the same specimen design is used to develop toughness for both virgin and precycled materials. Clearly, if the specimen design satisfied ASTM criteria for valid K_{Ic} for the virgin material, it will likewise satisfy those criteria for materials whose deformation response is unaltered by precycling or for materials that harden under the action of the preconditioning. However, if the materials cyclically soften, or otherwise soften under the action of some preconditioning, the initial specimen geometry may not satisfy the criteria that the thickness and crack length exceed $2.5\ (K_{Ic}/\sigma_{YS})^{\frac{1}{2}}$[10]. Indeed, increases in toughness would have to match or exceed decreases in yield strength to satisfy this condition. Otherwise, the results of tests on precycled specimens which soften represent values of toughness that tend to a

---

*** It is not artificial in the sense of constant amplitude load control used to develop the data. Indeed, increased softening or rougher fracture surfaces causes a decrease in growth rate for the same ΔK (not ΔK_{eff}). But it is artificial in variable amplitude service histories since the amount of closure depends on the wake of plasticity which depends on the load history. For this reason, closure that reduces growth rates in data development tests based on ΔK cannot be counted on for different load histories. Instead, data should be analyzed independent of closure effects, in terms of ΔK_{eff}.

plane-stress condition. If such is the case, the increase in apparent toughness is a result of comparing a valid K_{Ic} for virgin material with a plane-stress invalid toughness value. It has been known for almost two decades that plane stress values significantly exceed plane-strain values[10]****. The bottom line is that care must be taken to ensure an "apples" to "apples" comparison of toughness. Experiments must be designed and measurements must be made that permit valid toughness measurements.

The final study pertains to the influence of predamage on the subsequent crack-growth-rate of small pre-existing defects[22]. Specifically, the existing cracks are small, and not easily visible to the naked eye on mill surfaces. However, if the mill surface is removed and the surface viewed in oblique light, cracking is evident. The cracks of interest developed at outbent fibers that form along a longitudinal electrical resistance weld in a line pipe when the welding process went awry. Results of this study[22] showed that the multiply-initiated crack grew very quickly along the surface as the microcracks linked-up. Thereafter, the growth-rate dropped to match the behavior of a single long crack provided the correct aspect ratio was used in calculating ΔK. The conclusion was that initial microcracks could be treated as an equivalent initial flaw, and that their growth could be predicted using standard fracture mechanics methods just as would occur for larger initial cracks in preflawed virgin material specimens. In the present context this means that predamage in the form of "microcracked" material developed by fatigue precycling would behave in a manner similar to virgin material during the macrocrack growth phase of the life. Microcracking was accelerated as compared to virgin material, but only during a very small portion of the life during "link-up".

In view of the existing data, initial damage has an apparent influence on crack growth (threshold and finite growth rates) and fracture only as a consequence of changes in material flow behavior and exhaustion of ductility. Changes in flow behavior complicate comparison of virgin and precycled data because yield stress (1) influences crack closure and (2) alters the experimental conditions under which valid values of toughness can be

---

**** Plane stress and plane strain are idealized states that are only approached in structural metals in practical situations, particularly for plane strain.

obtained. Another factor that must be considered is the nature of the precycling--in most studies, precycling focused on the crack-tip region rather than the bulk material. The last factor of consequence is that the existing data do not include measurement of enough parameters to determine if changes in material or in testing conditions cause the apparent differences in cracking and toughness behavior.

The results of the literature review indicate that in order to determine whether the test conditions change or the steel's resistance changes, or both change (and how much), certain test types and parameters must be measured in specific test geometries.

First, if ASTM E399 is to be used to measure toughness, thicknesses and crack lengths must be chosen in anticipation of material properties after damaging. Cyclic deformation response must be determined to make such estimates. Alternatively, toughness can be developed using an inelastic test procedure such as ASTM E813[23] or by comparison of J-R curves. Even if these procedures are used, cyclic stress-strain data must be developed to interpret the results.

Second, for FCP testing, results in the literature show only a weak dependence of growth rate on the type of steel, microstructure, etc.[24] in the power-law growth regime. For this reason it is unlikely that hardening or softening would appreciably alter the growth rate--at least for long cracks. (Some question, however, exists as to the behavior of small cracks[25].) It appears that some analysis is necessary to sort out the significance of transient deformation response on growth rate. For a center cracked panel, LEFM analysis suggests:

$$r_p/a = (\sigma/\sigma_o)^2 \frac{1}{(2 - (\sigma/\sigma_o)^2)} \qquad (1)$$

where r_p is plastic zone size, a is semicrack length, σ is far field stress and σ_o is monotonic or cyclic yield stress, as appropriate. Defining the effective crack length as $a_e = a + r_p$, this analysis indicates that even at large values of r_p/a (beyond the limits of LEFM) growth rate is increased by only 12 percent for typical steels with a factor of 2 decrease in σ_o due to softening. Since (as noted earlier) a factor of 2 is typical for EH36 and HY80, the increase in growth rates due to softening will be modest at finite growth rates. However, at near-threshold conditions, the influence of transient response in changing

σ_0 may be significant, because of the dependence of closure on σ_0 as noted in earlier discussion.

In view of the above, the influence of changes in steels due to precycling may be most significant in the near-threshold regime so that this study of predamage effects should explore from the threshold up through finite growth rates. To emphasize the influence of predamage, the maximum predamage state that could reasonably develop in the absence of cracking or ahead of a crack that is removed in shipyard repairs should be considered. To allow isolation of the contributions of crack closure from changes in material flow behavior, measurements of crack closure should be made in addition to the usual crack growth parameters. To simulate the growth process in load-controlled ship structure, the crack growth should occur in an increasing K field. And, finally, because ships operate in an aggressive environment---sea water--often at low temperatures, consideration should be given to these parameters. In so doing, use should be made of a K-increasing threshold procedure to avoid the influence of calcareous deposits encountered in increasing-decreasing K tests (e.g., the current ASTM recommended practice for threshold) which may artificially arrest growth and give nonconservative threshold values.

4.a.2 Defining Cyclic (Fatigue) Predamage

This objective of this program focused on predamage prior to the appearance of visible cracks. Consequently, predamage sequences applied to precracked specimens, such as were just discussed, must be replaced by sequences which damage the material prior to cracking. The scope was restricted to sequences which damage otherwise "virgin" material at stresses below the yield prior to the formation of cracks.

One approach to predamage material would be to determine the fatigue life at some stress just below the yield and then impose a fixed number of cycles to predamage the material. However, given the scatter evident in fatigue lives approaching endurance limit stresses, this approach may, in some cases, lead to cracking and, in other cases, do very little damage. Thus, this approach is prone to significant scatter in the damage done. Furthermore, this approach does not permit direct measurement of the damage done.

A second approach would be to impose cycles on these materials and track their cyclic deformation behavior. Changes in deformation response are associated with microstructural changes leading to "damage" and eventual cracking[26,27]. That is, changes in the deformation response correlate with changes in damage so that the extent of damage can be defined as some prescribed change in deformation response. Such a definition of damage can be directly measured so that a given amount of damage could be repeatably imposed.

The second approach in which damage is defined as a change in deformation response was adopted because it offers a repeatable and quantifiable measure of the damage. This program's objective is best met under conditions which maximize predamage and therefore maximize the effect of predamage on toughness and crack propagation. Therefore, conditions which (1) cause the greatest change in deformation response without visible damage that (2) are imposed at a stress level below the yield stress are sought, as shown schematically in Figure 1.

It follows from Figure 1 that stress-strain curves which represent both monotonic and stable cyclic behavior are needed. The monotonic response is the usual "tensile" test data while the stable cyclic curve may be most easily found from an incremental step test[28].

4.a.3 Experimental Program and Data Analysis

The literature search indicates a program with the following scope of experiments and analysis is needed to meet the objectives.

- Incremental step cyclic loading of virgin material to determine the nature of the cyclic stress-strain curve and ductility at the extreme predamage condition.
- Precycling at just below the yield point to predamage but not crack the material.
- Fatigue-crack-growth tests on virgin material, focusing on the near-threshold conditions. Assess the role of closure.
  J_{IC} tests on specimens of virgin material that reflect the J history at the crack tip--useful in assessing the extreme effects

of predamage and in correlating the present study with the literature data.

- Fatigue-crack-growth tests on predamaged material, focusing on the near-threshold region--performed as for virgin material, with tests done under ambient conditions, and in aerated natural seawater at representative frequencies, including possible effects of closure.
- J_{Ic} tests on specimens of predamaged material.
- Comparison of toughness in terms of J_{Ic} to ascertain validity of predamaged toughness in terms of ASTM E399 requirements.
- Comparison of thresholds and growth rates to ascertain the influence of bulk predamage and crack tip predamage on growth rate under ambient and seawater conditions. Assess significance of closure for ship steels to see if future tests need consider this effect.
- Conclude concerning the significance of predamage and make recommendations as appropriate.

Table 1 summarizes the test matrix for this program. Note that predamage histories involve fully-reversed strain-cycling which induce fully-reversed stress-cycling that enhances the rate of cyclic-softening and develops a mean-stress-free predamage state. This develops damaged material that avoids an embedded mean-stress. Fatigue-crack-propagation (FCP) tests involve tension-tension load-cycling that helps reduce confounding crack-closure effects and avoids the need for buckling-guides that complicate environmental testing and some crack-measurement methods. Predamage, imposed at ambient conditions to simplify experimental procedures, is representative of typical marine service since the rate of cyclic softening is a very weak function of temperature over this limited temperature interval. Likewise, since the 50 percent fracture-appearance-transition-temperature is well below minimum service conditions for the steels examined, upper-shelf ductile toughness will be obtained over the range of service conditions and FCP will not involve related brittle-fracture mechanisms. Therefore, for the steels considered, testing at ambient conditions seems justified and representative of service situations. Finally, testing in seawater also will be done at ambient temperatures. This choice develops somewhat conservative data given the weak

temperature dependent increase in macrocrack growth rate in seawater or temperature increases over the range of interest in marine applications.

4.b. Materials and Specimens

The materials used in this study were a HSLA steel, ABS EH36, and a higher strength Q and T steel, HY80, in nominally half-inch thick plate obtained from ship plate suppliers to specifications set by the ABS[29] and the Navy[30], respectively. As evident in Tables 2 and 3, which are copies of the mill test reports, both materials met or exceeded the relevant specifications. Mechanical properties along the rolling direction for the EH36 indicated a yield of 400 MPa (58.1 ksi) and an ultimate strength of 511 MPa (74.2 ksi) with an elongation of 27 percent in 50.8 mm. The BHN for this material was 136 based on an average of 3 readings. Corresponding properties for the HY80 were a yield of 615 MPa (89.3 ksi), and an ultimate of 721.4 MPa (104.7 ksi), with an elongation of 32 percent in 50.8 mm. The BHN was 231 obtained as an average of 2 readings.

All specimens were cut with their long axis along the rolling direction (T-L orientation). Axial small diameter test specimens shown in Figure 2 were used to determine the monotonic and stable cyclic stress-strain behavior, as discussed in regard to Figure 1. Predamage of bulk material was done using panel specimens of the type shown in Figure 3. Buckling guides were used to restrain the specimen to inplane axial loading. Depending on the final use, the panel specimen was cut into J-toughness specimens or crack growth specimens, shown respectively in Figures 4 and 5. As detailed later, the multi-flawed specimen shown in Figure 5 was employed to maximize the amount of information that can be developed in the near-threshold regime during low-frequency testing in a seawater environment. Virgin material specimens also used these designs for both toughness and crack growth testing. The notch tips in crack growth specimens were made using EDM wire cutting with a 25 μm (0.001 inch) diameter wire at low power settings. The root radius was less than 25 μm (0.0001 inch) and the zone of damage to the microstructure was about 5 μm (0.0002 inch) deep. Since plane-strain fracture toughness could not be achieved in the 12.7 mm (1/2 inch) thick plate for these steels, K_{Ic} specimens were not used. Instead, K_{Ic} was estimated from J_{Ic} tests.

4.c. Experimental Set-Up and Procedure

All testing was done in commercially available closed-loop servo-hydraulic test systems. System load capacity was chosen to match the test purpose.

Bulk predamage was imposed in a 2225 N (500 kip) system under displacement control. This method leads to a symmetric load-drop that corresponds to the extent of cyclic softening and serves as the quantifiable measure of predamage. Displacement monitored over a 101.6 mm gage length along the edge of the test panel, using an ASTM Class B extensometer provided the control signal for these tests. Displacement was caused to follow a fully reversed sinusoidal wave form at a frequency of about 0.5 Hz. Load response was measured by a load cell mounted in series with the specimen. Cycling continued on each predamaged panel until the change in load corresponded to the preset damage level for that material, expressed in terms of a change in stress response (cf. Figure 1). Figure 6 is a photograph of this experimental set-up.

Deformation response tests done to establish the predamage level were performed in a 89 N system under axial-strain control. Load was measured by a load cell mounted in series with the specimen and used to calculate stress. Strain was controlled over the test section of the specimen shown in Figure 2 to follow an incremental step history of the type shown in Figure 7. This forcing function produces the monotonic response on the first excursion of the first block of cycles. The stable cyclic response is obtained from the locus of hysteresis loop-tips after several blocks of cycling led to stable (unchanging) stress-strain behavior. Cycling continued until stable behavior was observed. The set-up used for these tests is shown in the photograph in Figure 8. Testing and data analysis were done in accordance with ASTM E606 which standardizes such experiments.

Toughness testing and data analysis were done at ambient conditions in a 111.25 N system in accordance with ASTM E813 using the single specimen procedure. The specimen, shown in Figure 4, was set up for testing as shown in the photograph presented in Figure 9. Load was measured with a load cell mounted in series with load-pins, whereas load-point displacement was measured by a clip-gage mounted across projections machined in the crack mouth along the

load-line. Crack initiation and growth were monitored by the DC electric-potential-drop technique.

Crack growth rate testing was done in 111.25 N and 222.5 N test systems under load control to a sinusoidal forcing function through a load cell mounted in series with the specimen. All precracking was done in ambient laboratory conditions. For seawater tests, precracking continued in the seawater environment as the load-steps for the last several blocks of cycling were applied to move the largest flaw into the near-threshold regime. The number of load-steps prior to reaching the threshold for the first active flaw varied from 2 to 6. The frequency during precracking was 15 Hz for all specimens. Frequencies for ambient testing ranged from 5 to 15 Hz, whereas for seawater testing the frequency was fixed in a given test at 0.5 or 0.2 Hz. The load ratio, R_σ, in all tests was fixed at 0.01 (that is minimum load = 0.01 x maximum load) except for one test done at a ratio of 0.6. Crack closure was studied by the use of WA-type Micro Measurement® strain gages with an 1.63 x 1.63 mm grid mounted along but just below the potential crack path and by the LVDT mounted across the crack mouth. Closure is sensed by both techniques as a significant change in local compliance. The strain gages and LVDT were employed in the early tests which tracked cracking by KRAK® gages as the basis to calibrate the compliance at each potential crack path. A typical set-up for this test is shown in Figure 10.

Testing "in air" has been done in an ambient laboratory air environment controlled at 70F $\pm$ 2F and 50 percent relative humidity. Seawater testing was done at ambient temperature***** using small plexiglass chambers sealed to the specimen at each crack-line. The crack mouth was sealed through a compliant-material-seal wedged into the mouth but kept well away from the notch tip and the crack-tip region. The seawater testing was done with aerated natural seawater obtained from open waters near Battelle's Daytona Beach Facility. Seawater was received on a regular basis and changed out of the test chamber every week. Testing was done under free corrosion conditions. The pH of the water ranged from about 8.2 to 9.5.

***** As noted earlier, the choice of ambient temperature leads to slightly conservative FCP rate data for the range of temperatures of interest in marine applications.

The test procedures involved a K increasing history as illustrated in Figure 11. The increase in K due to a corresponding increase in load was followed by constant amplitude cycling to maintain the load-ratio constant throughout the test. With reference to Figure 5, note that the FCP test specimen has a series of flaws, each with a different length. Testing at a fixed load amplitude and load-ratio thus develops data that represent 6 different initial K levels and ΔK ranges that depend on the notch geometry. Provided that the notch tip is sharp and the notching method does not alter the local microstructure, cracking will occur quickly and grow beyond the zone of notch tip influence (order root radius/10). For the present work, the local EDM recast zone was about 5 μm deep, just slightly larger than the zone of influence of the notch which would be about 5 μm deep. The notch-tip was reasonably sharp, which, coupled with the local tensile residual stress in the notch field due to heat-sink around the recast zone, would produce expedient cracking once a notch was swept into the near-threshold regime. With this procedure, several K fields can be swept through the near-threshold K region before the largest initial K field produces a crack length that terminates the test. This approach therefore produces a range of data in the near threshold regime tied to less data at higher growth rates. Further details can be found in [31] which details the proof-of-concept for the procedure.

4.d. Measurement and Recording

Load and displacement were either measured or controlled and recorded in all tests. In the strain control tests to determine deformation response to set predamage conditions, stress calculated from load and area and strain calculated from displacement and gage length were recorded on an X-Y recorder. In the predamage panel test, displacement over the gage length was imposed to match the chosen predamage level and stress calculated from load and area was continuously monitored on a digital volt meter and recorded on a strip-chart until the predamage level was reached. For the J-R curve toughness testing, load-line displacement, load level, and crack length were recorded on analogue recorders as well as in digital form to be stored in a computer. The crack growth tests also used analogue and digital recording of load, local displacement and crack length based on KRAK® gage data, with the digital data

being stored in a computer. For the J-R and the fatigue crack propagation (FCP) tests, data stored digitally was subsequently dumped to diskettes for data analysis and plotting.

The FCP test records were regularly updated and the results plotted to decide whether to continue cycling at current load levels or to increase the load prior to further cycling to sweep another crack-tip into the near threshold domain.

5. EXPERIMENTAL RESULTS AND DATA ANALYSIS

5.a. Cyclic Deformation Behavior and Predamage Results

Monotonic and cyclic deformation behavior are shown in Figures 12a and 12b for the EH36 and HY80, respectively. The EH36 shows a decrease in stress response to cause a given strain--cyclic softening--at strains less than about 0.5 percent. At much higher strains the data for this material indicates that the stress required to cause a given strain increases slightly as compared to the monotonic behavior indicating slight cyclic hardening. In contrast to the EH36, the HY80 shows only the tendency to cyclic softening for the range of strains investigated. The extent of cyclic transient behavior observed for EH36 and HY80 is similar to literature data[20,32].

The data for the EH36 and the HY80 show that, at strains below the monotonic proportional limit, cycling causes initially linear-elastic response to develop cyclic plastic strain. That is, initially linear-elastic behavior tends to nonlinear or inelastic response. Consequently, cycling at design stresses considered to be linear-elastic may, after significant service, develop inelastic strains in material whose monotonic properties represent specified minimum levels. Examination of Figure 12 indicates that such inelastic behavior may develop at design stress levels, even for working stress designs with typical design factors of 0.6 applied to the specified minimum yield stresses (SMYS) (i.e., Fy = 0.6 SMYS), as is done in structural design codes[33]******.

****** Problems due to softening would, in practice, be limited to steels for which softening caused the yield to fall below 0.6 SMYS.

With reference to Figure 1 which defined the predamage state, the monotonic and cyclic data in Figures 12a and 12b led to the following predamage strains. For EH36, predamage is maximum at a target strain amplitude, $\Delta e/2$, of 0.212 percent for fully-reversed cycling. At this strain, the stress amplitude, $\Delta s/2$, may decrease to about 289.4 MPa (42 ksi). However, variability in that stress and the fact that cyclic softening tends to be exponential with cycles dictates a target softening level of 310 MPa. Similar consideration of the HY80 data led to targets of $\Delta e/2$ = 0.275 percent to a stress amplitude of 447.9 MPa (65 ksi).

Predamage of virgin material was done in bulk quantities for J-R specimens, since several CT samples could be cut from a predamaged panel. However, for fatigue crack propagation (FCP) specimens, each predamaged panel eventually became a FCP test sample. All predamage was done at 0.3 Hz in strain control. Three predamaged panels were needed for EH36 while four were needed for the HY80. As noted in Table 1, the predamaged panels for FCP were designated as EP1 and EP2 for the EH material and HP1, HP2, and HP3 for the HY material. The panels for J-R testing were designated as EJ1 and HJ1. Specific predamage conditions for these specimens were as follows.

Specimen Number	Actual $\Delta e/2$, Percent	Final $\Delta s/2$, MPa	Cycles Needed
EP1	0.235	305.2	340
EP2	0.212	310.0	260
HP1	0.278	448.0	720
HP2	0.275	445.0	728
HP3	0.275	445.0	727
EJ1	0.212	310.0	230
HJ1	0.275	448.0	500

Results of the predamage cycling show a similar number of cycles were required to achieve the target softened state. This consistency implies (1) that the initial mechanical properties of the panels probably did not vary

significantly and (2) that data developed from the various panels represents a common predamaged state.

5.b. J_{IC} and J-R Curves

Compact type specimens were fatigue precracked at the tip of the machined notches. The precracking for eight of the twelve specimens was carried out in accordance with the guidelines of ASTM E 813. The remaining four specimens (EH-3, EH-4, HY-3, and HY-4) were precracked at a load of about 0.6 of the limit load, which is higher than the 0.4 factor specified in E 813, to study the effect of a larger damage zone beyond the fatigue precrack on the fracture toughness. In all cases, the final fatigue precrack length was such that a/w was about 0.5.

All specimens were tested at a displacement rate selected to cause crack initiation in about 5 to 20 minutes. Data obtained were load (P), load-line displacement (LLD), and DC electric potential (U). Tests were terminated when the crack had extended by an amount equal to about 70 percent of the original ligament.

The onset of cracking was estimated from the DC electric potential data. To accomplish this, graphs of U versus LLD and U versus P were examined for points of slope change prior to maximum load. Engineering judgment then was applied to estimate U_o, the value of U at crack initiation. Crack growth beyond initiation was calculated from the ratio U/U_o using the Johnson expression[34]; the term for the spacing of the voltage probes (2y) in the Johnson expression was allowed to increase in proportion to the LLD as the test progressed. The final calculated crack extension and the final physical crack extension agreed within 4.5 to 13.1 percent; in each case, calculated values were less than actual values.

Deformation J (J_D) was calculated for each specimen. J_D was calculated in the manner specified in ASTM E 813-81 following the method developed by Ernst and Paris that takes into account crack growth[35]:

$$J_{D(i+1)} = [J_{D(i)} + (\frac{\eta}{b})_i (\frac{A_{i,i+1}}{B_N})] [1 - (\frac{\gamma}{b})_i (a_{i+1} - a_i)] \quad . \qquad (2)$$

The subscripts i and i + 1 relate to test record increments, and the parameters η, γ and b (defined below) are updated between each step.

$$\eta_i = 2 + 0.522\ b_i$$
$$\gamma_i = 1 + 0.76\ b_i$$
$$b_i = [w - (a_o + \Delta a)]$$

Full-range curves are presented in Figures 13 to 14, with the results of the J_{Ic} analysis shown in Table 4. All specimens met both the thickness and initial uncracked ligament criteria of E 813 for valid J_{Ic} (B or $b_o > 25J_Q/\sigma$ flow). The value of J_{Ic} was calculated using the J-Δa data that satisfy the E813 criteria for the linear regression line of the points on the J versus Δa plot between Δa of 0.15 mm and 1.5 mm offset lines, using the procedure set forth in E813.

The results from these tests show that, within the typical data scatter, there appears to be no significant effect of overload precracking or cyclic predamage on the J_{Ic} values. In addition, the full-range J-Δa curves are similar for each of the three conditions of each steel, with the exception of EH-PD specimens which did not achieve as high a J_{max} as the other four EH specimens. Since the value of J can be related directly to the Crack Opening Displacement (COD) parameter more commonly used in the offshore industry, it is expected that the effects of history sensed by J will also be evident in COD. (Generally, the value of J is numerically very much larger than the COD which may make detecting differences in toughness easier.) It is reasonably expected that conclusions drawn in regard to J_{Ic} would also be reached had COD been the basis for toughness measurement, all other factors being equal.

5.c. Fatigue Crack Propagation

As indicated in the test matrix presented in Table 1, data developed to characterize the FCP behavior represent several conditions. These conditions include the reference (as-received or virgin) state and the predamaged state, tested either in ambient conditions or in seawater at 23 C. Variations include stress-ratio, R, and frequency of cycling, f.

Data have been developed using compliance and KRAK® gage measurements of crack length, whereas crack-closure has been inferred through compliance measured in terms of crack-mouth-opening-displacement (CMOD) by an LVDT or by strain gages mounted adjacent to the crack-plane.

5.c.1. Measurement Methods and K Solution

Before presenting and analyzing the data, some comments on the measurement methods, the K solution, and the quality of the data are appropriate.

Compliance was considered as the basis to track both crack growth and crack closure. Compliance was the first choice to measure crack growth because, if successful, one technique could be used to make all crack growth/closure measurements.

The load-stepping procedure to develop growth rate data needed consistent, accurate growth measurements--such as had been obtained previously with KRAK® gages[31]. Thus, the accuracy of compliance in tracking crack growth was assessed by comparison of the compliance results with KRAK® gage data. The compliance of the cracked specimen has been determined assuming the cracks are plane fronted non-interacting symmetric double-edge-cracks in a tension panel. The value of a/w used represents the flaw of interest. Stress intensity factor solutions for edge-cracked panels[36,37] indicate that this assumption is viable within a 5 percent error for the placement of initial notch depths, until the longest crack grows to a length equal to 0.27 times the axial spacing of the cracks or until asymmetric growth at a dominant crack causes bending******* to interfere with the behavior of other cracks. Growth data have been edited accordingly.

For tests in air, the longest initial defect became the dominant crack, achieving a near critical length before the other cracks could develop. In all cases, growth of one crack of the crack-pair on each crack-plane created

---

******* Significant visual bending did not develop since the grips and load-train prevented it. However, very little bending across the crack plane is required to stop growth or be sensed on the "back-face" of the dominant flaw by an LVDT whose calibration is 1.25 μm equals 1 volt.

bending on that crack-plane. This bending eventually "shut-off" growth of the second crack, an interaction that was clearly evident on plots of load versus CMOD as an increase in apparent stiffness. These plots were used to identify when interaction began such that these data could be culled from the database during file-editing. Once a crack became dominant, it was treated as a single-edge-crack with bending restrained and an effective length of a/w. While the grips provided significant bending restraint, it is unlikely that full restraint was developed so that K may be underestimated for very large cracks ($a/w \geq 0.25$).

Typical crack growth features are illustrated in Figure 15 which shows a-N data for HP1. These results are used since this specimen had the most growth at flaws other than the dominant flaw and thus represents a worse-case for flaw interaction and problems in data interpretation. With the symbol code used in the figure, the shortest to longest initial flaws are HP1-2, 1, 6, 5, 4, 3, respectively. The figure shows that the most growth occurred for HP13--as expected since this is the longest flaw. Flaw 4 (HP14) opposite HP13 on the same crack-plane, however, did not follow the expected pattern. Instead, after some initial growth at increasing rates, the growth-rate trend reversed and the results remain in the scatter band for the shorter flaws. Examination of P-CMOD for these flaws shows that bending caused by the increase in the length of HP13 interfered with HP14, so that subsequent growth of HP14 was excised from the files used for data analysis. HP15 grew second longest even though this flaw, which lay on the same edge of the panel as HP13, was third longest initially. The length of this flaw increased more than 100 percent while HP13 increased about 700 percent. A strain-gage survey indicated that this significant growth upset the distribution of gross-section strains from the initial distribution by less than 5 percent at the crack-planes containing the active flaws. On this basis, the above assumption that each flaw can be treated initially as an independent pair of edge cracks with asymmetric growth seems viable, even for the extremes of growth developed in this study.

When the simple-slope growth-rate is determined for the a-N data in Figure 15 and plotted against the corresponding value of ΔK based on the assumed independent double-edge-flaw behavior, the trend shown in Figure 16 results. Note from this figure that the results for each flaw fall within a

rather tight continuous band from near-threshold rates up to the limit in ΔK that can be reasonably achieved with this test geometry. As can be seen from Figure 16, the trend from this test geometry merges with data for HY80 compact-tension (CT) specimens[38] cut from 1/2-inch plate and with wedge-open-loaded (WOL) specimens cut from 1-inch thick plate[39]. The continuity between data sets from the six flaws and with published data for other geometries at higher ΔK levels further supports the assumption that each flaw acts as an independent edge crack with asymmetric growth for the range of initial flaw sizes and growth behavior developed in this study.

Note from Figure 16 that a rather tight scatter-band develops even though growth rate is calculated on a simple-slope (point-to-point) basis and the data are unedited based on the increment of crack growth as compared to the measurement resolution. Such procedures often produce significant scatter. However, these procedures are retained because the already sparse data in the low-growth rate regime would be further reduced by editing and smoothing.********

It follows from the above discussion that the stress intensity factor, K, can be assessed reasonably using the double-edge crack equation at a given aspect ratio which, from handbooks (e.g. [36]), is given by

$$K = \sigma\sqrt{\pi a}\left\{(1+0.122\cos^4\frac{\pi a}{w})\left(\frac{w}{\pi a}\tan\frac{\pi a}{w}\right)^{\frac{1}{2}}\right\} \qquad (3)$$

This equation is considered useful within the just discussed constraints on data validity. Editing of raw crack-length versus cycles data limits the use of this equation to crack lengths less than 13.7 mm (0.54 inch) for nearly symmetric edge cracking, free of closure effects at one crack induced by the second crack on a given crack-plane.

The value of ΔK is simply the peak-to-peak value of K developed for the applied loading.

The theoretical compliance, λ, also can be obtained from handbook solutions for displacement, δ, at the plates edge[36] as:

******** Such tight scatter was not always observed, even for the data for a single flaw location. As expected, scatter could be reduced by editing on crack increment and using multiple-point procedures. These techniques were selectively applied to clarify some data trends.

$$\lambda = \delta t E' / P$$

$$= \frac{4Pa}{wtE'} V_1(a/w) \frac{tE'}{P} \qquad (4)$$

$$= 4\left(\frac{a}{w}\right) V_1\left(\frac{a}{w}\right)$$

where t = thickness, P = load, w = width, E'= plane strain corrected modulus of elasticity, and

$$(5) \quad V_1\left(\frac{a}{w}\right) = \frac{1}{\frac{\pi a}{w}} \left\{0.459\left(\sin\frac{\pi a}{w}\right) - 0.065\left(\sin\frac{\pi a}{w}\right)^3 - 0.007\left(\sin\frac{\pi a}{w}\right)^5 + \cosh^{-1}\left(\sec\frac{\pi a}{w}\right)\right\} .$$

Values of a/w which produced constant values of compliance were calculated and compared over a range of λ. For small a/w (the initial values) the theoretical and actual values of a/w compared within a few percent. However, beyond about 100 percent increase in crack length, the error between actual and theoretical crack length increased as a/w increased, probably because the theoretical compliance which represents symmetric growth ignores the bending which develops with asymmetric growth. An empirical expression of compliance based on actual data has been adopted and used up to the above noted limits on data acceptability associated with the K solution.

Differences between empirical compliance fitting constants for comparison specimens showed plus/minus errors typically less than a few percent--without a trend to increase as a/w increased within the just noted limits on data acceptance. Actual crack length was calibrated to local compliance using KRAK® gages. (KRAK® gages were successfully used to measure growth in developing the load stepping procedure[31] and in Battelle's participation in the NAVY round robin[38] for the ASTM crack growth in seawater). To maximize the accuracy of results, small KRAK® gages were used to capture the first 20 mm of growth. As the crack length approached the end of the gage, specimens were either regaged with bigger gages or the crack was tracked optically.

Compliance was measured at each flaw at the edge of the plate using a best-fit to 100 data pairs taken on the unloading load-displacement record from

3 successive cycles between 50 percent and 90 percent of the load range. The local displacement was measured using a spring-loaded short-stroke LVDT mounted on pivot-brackets. The LVDT was calibrated at 1.25 μm/volt (5×10^{-5} inch/volt) in a system with about 20 millivolts noise. Thus, the electrical resolution was about 0.025 μm displacement. This was well below the resolution of the KRAK® gage used for calibration which was about 10 μm, which sets the physical resolution of the LVDT-based compliance technique. The high level of electrical resolution was needed to minimize the number of cycles to produce a reasonably small increment of crack growth at low growth rates such that decisions regarding load stepping could be made. Calibration constants were determined to best-fit a compliance--crack length relationship using a third-order polynomial. Best-fit constants were determined for two ranges of crack size, and selected so as to give equal compliance and nearly equal first derivatives at the transition crack-length of 20 mm. The increment of growth between crack-length readings varied between 25 μm and 75 μm--well below the limit set by ASTM E647. However, these small increments were required to maximize the data developed as each flaw was swept through the near-threshold regime. Editing to increase this increment beyond the near-threshold regime was done in some cases, as discussed later.

5.c.2. Scatter and Growth Rate Transients

Variability in the crack growth measurement often can be traced to differences in growth rate behavior at opposite tips of a through crack or to differences in rate along the crack front. Differences in cracking rate may also develop when very little growth has occurred during the time that some preflaw develops a well defined front, with an established plastic zone and wake of plasticity from the preflaw.

Figure 17 shows a comparison of the cracking trends for EH material for both faces of the plate (tips of the crack). Note that the trends are similar and that cracking on one face (tip) does not lag or lead significantly. There was little curvature to the crack front, with less than 10 percent difference between mid-thickness and the average of the surface lengths. The similarity in crack growth across the thickness would suggest growth could be

tracked at one surface. Nevertheless, KRAK® gages were used for calibration on both faces for all flaws.

The results in Figure 17 represent a series of load steps as indicated by the + symbols located on the a-N trends. To avoid confusion caused by growth rate transients due to load steps designed to sweep flaws through or beyond the threshold, the load has been increased slowly at a rate of dK/dN of about 3×10^{-3} MPa $\sqrt{m} \cdot cycles^{-1}$. The load on the specimen represented here was stepped from 50.64 N (11.38 kip) through 6 steps to 64.04 N (14.39 kip), but the a-N trend is continuous with little or no evidence of transients in growth rate at a load step. This suggests that the dK/dN rate used significantly reduced the expected transient behavior. Because the scale used in Figure 17 may mask what transients occur, the average of the growth rate trend for the data in Figure 17 has been replotted in Figure 18. Figure 18 uses a different symbol for each load step and resets the cycle-count to zero with each load step. Replotted this way, these data still do not show any obvious transients due to load steps. As is evident in Figure 16, transients do not appear when these data are plotted on da/dN - ΔK coordinates: instead, Figure 16 shows a tight scatter band in rate, except for the tail at lower rates tending toward the threshold.

Differences in K-history and environment also may alter the conclusion that significant transients due to load stepping have been avoided. Accordingly, results for the seawater environment with different load levels and steps have been examined. Typical a-N results are shown in Figure 18, in a format identical to Figure 17. These results also support the conclusion that the load-stepping procedure does not introduce significant artificial transients in the growth trends.

It follows that the FCP analysis procedures develop reliable data over the range of parameters studied and that the test method does not develop artificial trends due to transients. Scatter or bias related to measuring cracks at the surface seems to be well within typical results. The assumption that each flaw behaves independently as an edge crack seems justified by the continuous data trends for the range of flaws studied and the fact that trends for the dominant crack merge into literature data. Growth rates for all flaws define a near-threshold trend within a narrow scatter band (c.f. Figure 15). Thus, the trend developed is a measure of near-threshold behavior rather than a

start-up behavior that otherwise would be excised from test records per ASTM E647.

5.c.3. da/dN - ΔK Results

Reference (As-received) Material. Figures 19a and 19b present the da/dN-ΔK behavior for the as-received material, in air at 23 C at a stress ratio R = 0.01 (so $K_{max} \cong \Delta K$) for EH36 and HY80, respectively. Results presented for EH36 represent two specimens, EF1 and EF2, and cover growth rates from less than 10^{-10} m•cycle^{-1} (about 10^{-9} inch•cycle^{-1}) to about 10^{-7}m•cycle^{-1}. These data merge with CT specimen data[31] and center-cracked panel (CCP) data[20] for higher growth rates. These data indicate a threshold of about 4 MPa•m$^{\frac{1}{2}}$, consistent with a "long crack" threshold from CT data and earlier developed data using the load-stepping procedure[31]. Results for HY80 representing one specimen, HF1, cover a rather small span of growth rates because of experimental difficulties. These data blend in with data from a variety of sources[38-41] for CT, CCP, and WOL specimens cut from 12.7 mm and 25.4 mm thick plate and several thinner specimens. The threshold for these data is estimated at about 7MPa•m$^{\frac{1}{2}}$, a value comparable to literature data[42] for similar classes of steel.

The effect of mean stress was explored by one test of HY80 material: specimen HF2 was tested at R = 0.6. Figure 20, parts a, b, and c, presents the data for HF2 on coordinates of growth rate versus ΔK, K_{max} and $K_{max}\sqrt{1-R}$[43]. On da/dN -ΔK coordinates the growth rate at R = 0.6 lies above the trend for R = 0 , similar to the literature trend[44] reproduced in Figure 20d. As expected, the higher mean stress enhances growth rate when data are compared at equal ranges of K. In contrast, on coordinates of da/dN - K_{max} the growth rate for R = 0.01 lies above that for R = 0.6, because for the same K_{max} the range of K is larger at R = 0.01. Finally, when a parameter to account for stress ratio is used--$K_{max}\sqrt{1-R}$--the growth rates are consolidated reasonably.

Predamaged Material. Results for samples of predamaged material, tested at R = 0.01 in air at 23 C, are plotted on coordinates of da/dN and ΔK for EH36 and HY80 in Figures 19c and 19d, respectively. Results for EH36 developed from EP1 cover rates from about 10^{-11} m•cycle^{-1} to more than 10^{-6} m•cycle^{-1}. The data for predamaged EH36 material imply little difference in FCP at finite growth

for predamaged EH36 material imply little difference in FCP at finite growth rates as compared to virgin material. However, the threshold seems to be somewhat higher than for the as-received material. The trend at higher growth rates matches the virgin material, merging with literature data noted in regard to Figure 19. In the near threshold regime, the threshold trend for HY-80 seems to develop at higher ΔK levels than it did for as-received material, similar to the behavior shown by the EH36.

Seawater Results for EH36. Seawater FCP is shown for EH36 tested at 23 C and R = 0.01 at a frequency of 0.5 Hz in Figures 21a and 21b for as-received and predamaged material, respectively. Data for EF3 represent as-received material and cover a range in rates from 10^{-10} m•cycle^{-1} to near 10^{-6} m•cycle^{-1}. Results for EP2 represent predamaged material and span a slightly greater range of rates at both extremes. Comparison of the seawater data with the ambient trends presented in these figures shows finite growth rates are similar to slightly increased as compared to the corresponding ambient results. However, the near-threshold conditions develop at slightly higher ΔK values in seawater as compared to air. Slight increases in growth rates up to factors of 2 are common in the literature for steels at tested finite growth rates in saltwater/seawater[42], so the behavior observed is consistent with the literature. The trend to higher thresholds represents a condition for which little data exists. The limited data for other steels do show this trend, with slightly higher thresholds and the same crossing tendency to higher growth rates at higher values of ΔK (e.g.,[45]). This tendency to higher thresholds may be expected at low levels of CTOD, since local closure caused by corrosion debris can "prop-open" the crack thereby reducing the effective stress intensity range. The predamaged material shows the biggest reduction on the threshold, and even bigger effects may be seen at lower frequencies.

Seawater Results for HY80. FCP in seawater is shown for HY80 tested at 23 C and R = 0.01 at a frequency of 0.5 Hz in Figures 22a and 22b, respectively. Results for identical conditions, except that the frequency was 0.2 Hz, are shown in Figure 22c. The results for HY80 show the same patterns in da/dN - ΔK that were developed in the EH36. The reference virgin material shows little change in the near-threshold regime, with an increase in growth rate developing

increased threshold, with a x3 to x5 increase in growth rate at higher ΔK values. Reducing the frequency to 0.2 Hz causes a further increase in the threshold and a x3 to x5 increase in da/dN at higher values of ΔK.

Crack closure and da/dN-ΔK_{eff} Results. The phenomenon of crack closure was identified as a significant factor in FCP in the early 1970's. Elber[46] argued that a crack could not grow unless the crack-tip was open, and introduced the notion of the effective stress intensity factor range, ΔK_{eff}, defined as

$$\Delta K_{eff} = \frac{P_{max} - P_{open}}{P_{max} - P_{min}} \Delta K; \text{ when } P_{open} > P_{min} \qquad (6)$$

$$\Delta K_{eff} = U \Delta K$$

where P_{max}, P_{open} and P_{min} are the maximum, opening and minimum loads and ΔK is the peak to peak value of K as defined earlier. When closure occurs, $P_{open} > P_{min}$ so that $\Delta K_{eff} < \Delta K$.

For the present study, closure has been assessed in terms of the load versus CMOD behavior, supplemented by strain gages along the crack line. Details of related techniques are well established[47,48]. Suffice it for the present to illustrate a typical example, as shown in Figure 23. When $P < P_{open}$ note that the stiffness, P/CMOD, represents unloading of the crack faces. Once $P > P_{open}$, the stiffness is the inverse of the local compliance used to track crack growth.

Plots similar to Figure 23 were made at regular cycle intervals for each of the flaws. It was found that closure was not a factor, within the sensitivity of the CMOD system and autographic recording devices used, for the "in-air" data for the reference materials. Two factors contribute to the absence of closure in these tests: low stress and positive stress ratio.

Normalized with respect to the yield stress of the materials, σ_o, the ratio of the applied (gross) stress, σ, to σ_o, (that is σ/σ_o), was quite low. For EH36, values of σ/σ_o ranged from 0.09 when cracks were small, and increased to 0.19 after incrementing the load as the largest cracks grew longer. Corresponding values for the HY80 were 0.06 and 0.13, respectively. Plane

stress plastic zone sizes ranged from about 7 μm initially to about 125 μm as the tests finished.

The small initial plastic zone means that there is little inelastic stretch in the wake of the crack. This factor when coupled with the second factor--the stress ratio of 0.01 which does not promote closure as would negative stress ratios--means that there is little tendency for closure under initial conditions for the in-air tests. With increased crack length and plastic zone size, the corresponding increased compliance and larger CMOD (CTOD) accommodates the increased crack-tip stretch in the wake of the crack so that, again, closure fails to develop as the crack grows.

The extent to which closure develops depends on how well the CTOD accommodates changes that develop propping at the crack tip, such as would be caused by plastic stretch due to FCP and corrosion debris. The crack tip opening displacement, CTOD, can be estimated as[49]:

$$\text{CTOD} = C_1 \frac{K^2}{\sigma_o E} \quad , \tag{7}$$

which at threshold in the EH36 (~4 MPa•m$^{\frac{1}{2}}$) is about 0.39 μm for $C_1 \cong 0.5$[49]. The corresponding value of CTOD for HY80 is about 0.24 μm for its slightly higher threshold of about 6 MPa•m$^{\frac{1}{2}}$. That is, based on "virgin" properties under otherwise similar near-threshold conditions, the crack tip opening displacement is almost 1.6 times greater in EH36 than in HY80.

These results imply that the EH36 could accommodate up to 1.6 times more "wedging" at the crack-tip--due, for example, to increased inelastic stretching during FCP, or debris build-up from corrosion--before the crack-tip in EH36 developed closure conditions like those in the HY80. If predamage mechanical properties are used for σ_o to represent the situation for predamaged material, the difference between CTOD for the EH36 and HY80 at near-threshold conditions decreases from 1.6 times to 1.38 for a 0.2 percent offset σ_o, and to less than 1.1 for σ_o based on a proportional limit. That is, because the CTOD in both materials is similar, after the effect of predamage (manifest as changes in σ_o) is accounted for, there is little difference in the crack-closure characteristics of these two steels.

Consider now how predamage influences the crack-tip plastic-zone size, which relates to the local inelastic stretch during crack growth and that in turn develops the wake of plasticity due to crack growth. Recall that the EH36 cyclically softens to a proportional limit of about 206 MPa. This softening produces an increase in the plastic zone size of about 4 times that in the virgin material. Softening in the HY80 likewise produces an increase in plastic zone size; however, the plastic zone size in the virgin HY80 material is only about 45 percent of that in the virgin EH36. For this reason, predamage of EH36 is expected to produce about a factor of 2 bigger increase in the inelastic stretch during FCP than would develop in the HY80. Thus, the EH36 may develop closure in the predamaged material whereas the HY80 may not.

As noted above, the CTOD levels for predamaged EH36 and HY80 were similar, so that a comparable build-up of corrosion debris could be expected to develop similar levels of closure in predamaged material. In contrast, the differences in CTOD for virgin HY80 and EH36 implies that a comparable build-up of debris could produce more closure in the HY80 material. While the effects of predamage-induced-plasticity on closure could be explored through the dependence of σ_0 on the predamage history, the effect of debris on closure cannot be analyzed so directly. Projections of closure due to debris are uncertain since analyzing the development and packing of corrosion debris is unreliable, if not impossible. Suffice it to note that closure can be expected to develop due to corrosion debris, provided the layer of debris is on the order of the CTOD.

As anticipated in view of the above, tests on predamaged EH36 and all seawater experiments showed evidence of significant closure. Because closure did not develop at similar loads in the in-air tests, except for the predamaged EH36, this closure can be associated with the corrosion process. Figure 24 parts a and b plots the ratio U in Equation 6 as a function of K_{max} for the EH36 and the HY80 seawater tests. At lower levels of K_{max} there is limited closure, and as K_{max} increases closure develops further, as indicated by further decreasing values of U. At still higher levels of K_{max} the tendency for closure decreases as values of U increase back toward unity. This decrease in closure effects at higher values of K_{max} is driven by the corresponding increase in compliance for longer cracks for which the crack-tip stretch increases faster than the thickness of the corrosion deposit.

The closure trends in Figure 24 are similar to results for other steels, as, for example, the work of Endo et al[50]. They show that closure develops very quickly after immersion and present similar trends for decreasing U with increasing K_{max}. As with the present data, K_{max} does not correlate their data for different ΔK histories. This is not surprising in that the development of the corrosion debris producing closure is dependent, at least, on the rate new surface is exposed and the accessibility of the environment to the crack-tip. In contrast, the local stretch or crack-tip opening displacement which accommodates this debris depends on K_{max}. Since both the production of debris by corrosion processes and the accommodation of debris by the CTOD are not both related uniquely by K_{max}, different K histories will produce different U histories, that generally will not be correlated by K_{max}.

da/dn-K_{eff} Results. Given the significant closure evident in Figure 24, the da/dN-ΔK trends discussed earlier will differ when evaluated in terms of ΔK_{eff}, particularly at K_{max} levels greater than about 7MPa·$m^{\frac{1}{2}}$. The FCP data discussed earlier in regard to Figures 19-22 have been plotted on coordinates of da/dN and ΔK_{eff} in Figures 25 to 28.

There are two significant changes in the patterns noted earlier when closure is accounted for. First, on da/dN-ΔK coordinates results for the predamaged materials, as well as results for seawater, showed thresholds generally above the reference condition whereas now there is little or no difference. Differences when closure is accounted for are within about 10 percent, and may indeed be smaller with better resolution of closure. Second, because of the apparent increase in threshold as compared to the reference condition when data are viewed on da/dN-ΔK coordinates, FCP trends for seawater tests cross the ambient trend on da/dN-ΔK whereas this does not occur if ΔK_{eff} used. As when ΔK is used, the use of ΔK_{eff} indicates that seawater enhances FCP rates more so for the slowest frequency, consistent with literature trends[42]. Finally, predamaged material behaves the same as virgin material when closure is accounted for. This, too, is consistent with literature data for other materials that shows a common near-threshold trend for a variety of material conditions that otherwise produce a range of thresholds when analyzed using ΔK[51].

It should be emphasized that the wake of plasticity in ambient tests at a fixed stress ratio will produce a unique level of closure only so long as the remaining ligament in the specimen is very large as compared to the crack length and the crack's plastic zone size. This unique level of closure leads to a unique threshold ΔK which is a function of stress ratio. However, if the remaining ligament becomes small compared to the crack length (i.e., the elastic stress field that confines the wake of plasticity is no longer dominant), the value of U becomes non-unique. The value of U also becomes non-unique if the ratio σ/σ_0 is large or the plastic zone size becomes large compared to the crack length. These situations violate limitations for valid applications of LEFM, producing non-unique thresholds because the crack-closure behavior (U) is no longer unique. The closure situation under ambient conditions is further complicated by corrosion debris and deposits[52] in marine applications. For these reasons, care must be taken in adapting laboratory FCP data to design.

Thresholds found in laboratory tests are only useful if the ΔK history and wake of plasticity that occurs in the laboratory test also develop in the same way in the design application. Particular attention must be paid to σ/σ_0--this value is typically much larger in design applications with physically small cracks than it is in FCP tests with 40 to 50 percent of the ligament cracked. Attention must also be paid to the type of loading. Stress ratios and stress levels in laboratory tests are held constant--however, they vary in practice and so may alter closure levels in practical applications. Finally, laboratory specimens are designed to develop reproducible data and do so in regard to the wake of plasticity and closure because the elastic field surrounding the wake remains fully effective. Unrestrained out-of-plane deformation, either in tension or compression, is common in many structures once a crack disturbs the load transfer assumed in design. If this occurs, there may be no unique wake of plasticity and closure may not develop--making use of a threshold in practical applications tenuous. From the designer's viewpoint, the safest approach is to ignore the threshold and use a back extrapolation of the growth rate trend at finite rates. This also provides a safe approach in dealing with the problem of short cracks which tend to grow at ΔK levels less than the threshold, in part because of differences in crack closure (e.g., see [53]).

6. SUMMARY AND CONCLUSIONS

Experiments designed to investigate whether cyclic loading prior to the formation of fatigue cracks develops predamage that alters the inherent toughness and FCP behavior of EH36 and HY80 have been developed, along with a predamage method that can be quantified. Results have been analyzed to assess whether apparent effects of predamage are due to inherent changes in the material or are a consequence of the influence of predamage on test method itself. Plasticity that develops during cycling at strains less than the monotonic proportional limit was identified as a consequence of damage and the associated change in stress response (cyclic softening or hardening) was adopted as a measure of damage. Material was predamaged in bulk form to a prescribed level measured by the change in stress for a given total strain and samples for fracture toughness tests and fatigue crack propagation (FCP) tests were cut from this bulk predamaged material. Standard fracture toughness tests and FCP tests were then performed on virgin material and predamaged material covering a range of test conditions. The extent of predamage effects was then judged by comparing virgin and predamaged material data trends.

Conclusions reached as a result of this study follow for the range of materials and the conditions considered, taken with reference to virgin material under ambient conditions.

- The fracture toughness and FCP behavior developed in this study are consistent with literature trends for virgin materials.
- Predamage does not alter the toughness when toughness is judged using a method that accommodates plasticity (e.g., J_{Ic}).
- If predamage hardens materials appreciably, the dynamic toughness may be reduced as compared to virgin material.
- Predamage produces an apparent increase in the threshold for FCP when analyzed using ΔK (or K_{max}).
- Beyond the near-threshold regime, the FCP behavior is not altered by predamage when analyzed using ΔK (or K_{max}).
- Testing in seawater produces an increase in the threshold as compared to ambient conditions when analyzed using ΔK (or K_{max}).

- Beyond the near-threshold regime, the FCP behavior in seawater produces cracking at rates 2 to 5 times that in ambient conditions when analyzed using ΔK (or K_{max}).
- Predamage does not alter the FCP behavior when closure is accounted for using ΔK_{eff}.
- Testing in seawater produces a threshold at or slightly less than for ambient conditions when closure is accounted for using ΔK_{eff}.
- Decreasing the frequency from 0.5 Hz to 0.2 Hz increases the growth rate from the near threshold regime through finite growth rates, causing a slight reduction in the threshold.
- Designs based on a ΔK_{eff}-based data format reasonably represents the FCP behavior for virgin and predamaged steels for the steels and material conditions considered.

7.0 REFERENCES

[1] I. Roman, et al, "The Effect of Cyclic Loading on the Apparent Cleavage Fracture Toughness of 1Cr-Mo-V Rotor Steel", Technical Report, EPRI NP-1023, March, 1979.

[2] R. O. Ritchie and J. F. Knott, in Mechanics and Mechanisms of Crack Growth, Proceedings British Steel Corporation Conference, Cambridge, pp. 201-225, April, 1973.

[3] C. J. Beevers, et al, Metal Science, 9, pp. 119-126, 1975.

[4] W. F. Brown, Jr. and J. E. Srawley, "Review of Developments in Fracture Toughness Testing", American Society for Testing and Materials, ASTM STP 463, Philadelphia, pp. 228-231, 1970.

[5] J. G. Kaufman and P. E. Schilling, "Influence of Stress Intensity Level During Fatigue Pre-Cracking on Results of Plane-Strain Fracture Toughness Tests", American Society for Testing and Materials, ASTM STP 536, Philadelphia, pp. 312-319, 1973.

[6] I. Roman and K. Ono, Model for Fracture Toughness Alteration Due to Cyclic Loading, International Journal of Fracture, 19, pp. 67-80, 1982.

[7] J. J. May, "British Experience with Plane Strain Fracture Toughness (K_{IC}) Testing", American Society for Testing and Materials, ASTM STP 463, Philadelphia, pp. 41-62, 1970.

[8] G. J. Fowler, "Fatigue Crack Initiation and Propagation in Pearlitic Rail Steel", Ph.D. Thesis, Materials Department, University of California, Los Angeles, 1976.

[9] J. E. Srawley and W. Brown, Jr., "Fracture Toughness Testing and its Applications", American Society for Testing and Materials, ASTM STP 381, 1965.

[10] Anon, "Standard Test Method for Plane-Strain Fracture Toughness of Metallic Materials", American Society for Testing and Materials, ASTM E399, 1983.

[11] Anon, "Standard Test Method for Constant-Load-Amplitude Fracture Crack Growth Rates Above 10^{-8} m/cycle", American Society for Testing and Materials, ASTM E647, 1983.

[12] V. T. Troschchenko and V. V. Pokrovskii, "Fracture Toughness of Structural Alloys Under Cyclic Loading, Communication 1", Strength of Materials, Vol. 15, pp. 735-742, June 6, 1983.

[13] V. T. Troschchenko and V. V. Pokrovskii, "Fracture Toughness of Structural Alloys Under Cyclic Loading, Communication 2", Strength of Materials, Vol. 15, pp. 743-750, June 6, 1983.

[14] N. E. Dowling, "Fatigue-Crack Growth Rate Testing at High Stress Intensities", American Society for Testing and Materials, ASTM STP 631, pp. 139-158.

[15] N. E. Dowling to B. N. Leis of Battelle, Private Communication, March, 1984.

[16] J. D. Landes and T. R. Leax, "Load History Effects on the Fracture Toughness of a 4340 Steel", American Society for Testing and Materials, ASTM STP 833, pp. 436-448, 1984.

[17] W. G. Clark, Jr., "Effect of Cold Working on K_{ISCC} in a 4340 Steel", Flaw Growth and Fracture, American Society for Testing and Materials, ASTM STP 631, pp. 331-344, 1977.

[18] W. W. Gerberich and N. R. Moody, "A Review of Fatigue Fracture Topology Effects on Threshold and Growth Mechanisms", Fatigue Mechanisms, Proceedings of an ASTM-NBS-NSF Symposium, Kansas City, Missouri, May, 1978, J. T. Fong, Editor, American Society for Testing and Materials, ASTM STP 675, pp. 292-341, 1979.

[19] H. Abdel-Raouf, Ph.D. Thesis, University of Waterloo, 1972.

[20] B. N. Leis, et al, "Fatigue Strength of Great Lakes Ships - Phase I and Phase II", Battelle Reports to American Bureau of Shipping, 1979 and 1982.

[21] Private Communication with Earnie Czyryca of David Taylor Naval Ship Research and Development Center, April, 1984, and data in Materials Properties Data Center Handbook for HY80 (MPDC is maintained by Battelle).

[22] "ERW Weld Zone Characteristics", Final report from Battelle to American Gas Association, AGA Report 130, Catalog L51427, 1982.

[23] Anon, "Standard Test Method for J_{Ic}, A Measure of Fracture Toughness", American Society for Testing and Materials, E813, 1981.

[24] S. T. Rolfe and J. M. Barsom, "Fracture and Fatigue Control in Structures", Applications of Fracture Mechanics, Prentice-Hall, Inc.

[25] B. N. Leis, M. F. Kanninen, A. T. Hopper, J. Ahmad, and D. Broek, "A Critical Review of the Short Crack Problem in Fatigue", AFWAL-TR-83-4019, January, 1983.

[26] S. Kocanda, "Fatigue Failure of Metals", Sijthoff & Noordhoff, 1978.

[27] M. Klesnil and P. Lukas, "Fatigue of Metallic Materials", Materials Science Monographs, 7, Elsevier, 1980.

[28] J. Morrow, "Cyclic Plastic Strain Energy and Fatigue of Metals", Internal Friction, Damping, and Cyclic Plasticity, American Society for Testing and Materials, ASTM STP 378, pp. 45-84, 1965.

[29] Anon, "rules for Building and Classing Steel Vessels", American Bureau of Shipping, 1978.

[30] Anon, Military Standard: MIL S-16216J, HY80-TY.1.

[31] B. N. Leis, "Validation of an Expedient Method for Generating Threshold Fatigue Data", Final Report to Corporate Technical Development, Battelle Memorial Institute, 1984. (Available upon request.)

[32] S. I. Kwun and M. E. Fine, "Fatigue Macrocrack Growth in Tempered HY80, HY130, and 4140 Steels: Threshold and Mid-ΔK Range", Fatigue of Engineering Materials and Structures, Vol. 3, No. 4, pp. 367-382, 1980.

[33] Anon, American Institute of Steel Construction Structural Steel Design Code.

[34] K. Schwalbe and D. Hellman, "Application of the Electric Potential Method to Crack Length Measurements Using Johnson's Formula", Journal of Testing and Evaluation, Vol. 9, No. 3, pp. 218-221, May, 1981.

[35] H. A. Ernst and P. C. Paris, "Technique of Analysis of Load-Displacement Records by J-Integral Method", U. S. Nuclear Regulatory Commission Report, NUREG/CR-122, January, 1980.

[36] H. Tada, P. C. Paris, and G. R. Irwin, The Stress Analysis of Cracks Handbook, Del Research Corporation, Revised, 1977.

[37] D. P. Rooke and D. J. Cartwright, "Compendium of Stress Intensity Factors,", HMSO, 1976.

[38] R. Rungta and B. N. Leis, Corrosion Fatigue of HY80 in Saltwater; Navy/ASTM Round Robin, T. W. Crooker, Coordinator, 1982.

[39] J. M. Barsom, E. J. Imhof, and S. T. Rolfe, "Fatigue-Crack Propagation in High Yield-Strength Steels", Engineering Fracture Mechanics, Vol. 2, pp. 301-317, 1971.

[40] P. M. Scott, "Chemistry Effects in Corrosion Fatigue", in Corrosion Fatigue: Mechanics, Metallurgy, Electrochemistry, and Engineering, American Society for Testing and Materials, ASTM STP 801, pp. 319-350, 1983.

[41] J. Congleton, H. Craig, B. K. Denton, and R. N. Parkins, "Crack Growth in HY80 and HY130 Steels by Corrosion Fatigue", Metal Science, Vol. 13:7, pp. 436-443, July, 1979.

[42] C. E. Jaske, J. H. Payer, and V. S. Balint, "Corrosion Fatigue of Metals in Marine Environments", Metals and Ceramics Information Center (MCIC 82-42), Battelle Press, 1981.

[43] E. K. Walker, in Effects of Environment and Complex Load History on Fatigue Life, American Society for Testing and Materials, ASTM STP 743, pp. 553-575, 1981.

[44] W. H. Hartt and J. H. Adamson, "Fatigue and Corrosion Fatigue of HY80 Steel, as Applicable to Anchor Bolt Failures", Final Report, Contract N00014-78-C-0307, ADA072067, July, 1979.

[45] O. Vosikovsky, "Effects of Stress Ratio on Fatigue Crack Growth Rates in X70 Pipeline Steel in Air and Saltwater", Journal of Testing and Evaluation, Vol. 8, No. 2, pp. 68-73, March, 1980.

[46] E. Elber, "The Significance of Fatigue Crack Closure", in Damage Tolerance in Aircraft Structures, American Standards for Testing and Materials, ASTM STP 486, pp. 230-24, 1971.

[47] J. M. Baik and R. J. Asaro, "Fatigue Crack Growth and Overload Retardation in 2048 Aluminum", in Mechanics of Fatigue, American Society of Mechanical Engineers, ASME AMD-Vol. 47, pp. 33-52, 1981.

[48] N.J.I. Adams, "Fatigue Crack Closure at Positive Stresses", Engineering Fracture Mechanics, Vol. 4, pp. 543-554, 1972.

[49] J. F. Knott, "Fundamentals of Fracture Mechanics", John Wiley & Sons, 1973.

[50] K. Endo, K. Komai, and T. Shikida, "Crack Growth by Stress-Assisted Dissolution and Threshold Characteristics in Corrosion Fatigue of a Steel", in Corrosion Fatigue: Mechanics, Metallurgy, Electrochemistry, and Engineering, ASTM STP 801, pp. 81-95, 1983.

[51] R. J. Bucci, "Effect of Residual Stress on Fatigue Crack-Growth-Rate Measurement", ASTM STP 743, pp. 28-47, 1981.

[52] R. Murakami and W. G. Ferguson, "The Effects of Cathodic Potential and Calcareous Deposits on Corrosion Fatigue Crack Growth Rate in Seawater for Two Off Shore Steels", Fatigue of Engineering Materials and Structures, Vol. 9, No. 6, pp. 477-488, 1987.

[53] B. N. Leis, et al, "Critical Review of the Fatigue Growth of Short Cracks", Engineering Fracture Mechanics, Vol. 23, No. 5, pp. 883-898, 1986.

TABLE 1. TEST MATRIX

Test Type	Material	
	EH36	HY80
Damage Levels (ambient)		
Monotonic tension	ET3,4	HT1,2
Cyclic σ-ϵ	ET1,2	HT3,4
Predamage Panels (ambient)		
FCP	EP1, EP2	HP1, HP2, HP3*,
J-R	EJ1	HP4, HJ1*, HJ2
J-R/J_{Ic} (ambient)		
Virgin	EH2-5	HY1-4
Predamaged	EHPD1,2	HYPD1,2
FCP (ambient and seawater)		
Virgin, ambient, R=0.01	EF1, EF2	HF1
Predamaged ambient, R=0.01	EP1	HP1
Virgin ambient, R=0.6	--	HF2
Virgin seawater, R=0.01, f=0.05Hz	EF3	HF3
Predamaged seawater, R=0.01, f=0.05Hz	EP2	HP2
Predamaged seawater, R=0.01, f=0.2Hz	--	HP4

*Samples remade because of test control problems.

TABLE 2. MILL REPORT FOR EH36

ARMCO . nco Steel Corporation
P.O. Box 88120, Houston, Texas 77015

MILL REPORT
572-1000-9-25-78

"THIS CERTIFIED TEST REPORT HAS BEEN DELIVERED TO A CONSIGNEE OF MATERIAL PURCHASED FROM ARMCO STEEL CORPORATION TO BE THE POSSIBILITY OF ITS REMOVAL OR THE DELIVERY OF THIS REPORT TO A PARTY IS MUST BE RE- CERTIFIED BY AND UNDER THE NAME OF SUCH CONSI- -EE"

PAGE 1 OF 1

JOB, CONTRACT NO

SOLD TO
AMERICAN BUREAU OF SHIPPING
ATTN: S G STIANSEN - V.P.
OCEAN ENGINEERING DIV.
45 BROAD ST.
NEW YORK NY 10004

SHIP TO
AMERICAN BUREAU OF SHIPPING
% BATTELLE COLUMBUS LABS
505 KING AVE.
ATTN: DR. DAVE BROEK
COLUMBUS OH 43201

PURCHASE ORDER DATE	PURCHASE ORDER NUMBER	
09/05/78	VERBAL TO GEK	
SHIPPER NO	REC ORDER NO	DATE SHIPPED
7049052	THS0727	09/22/78
VEHICLE IDENTIFICATION		
YELLOW	1	TRUCK

MAIL TO
AMERICAN BUREAU OF SHIPPING
ATTN: S.G. STIANSEN - V.P.
OCEAN ENGINEERING DIV.
45 BROAD ST.
NEW YORK NY 10004

000117861-7014 LA 79

THE CHEMICAL, PHYSICAL OR MECHANICAL TESTS REPORTED HEREIN ARE CORRECT AS CONTAINED IN THE RECORDS OF THE CORPORATION

SIGNED _____ METALLURGIST DEPT

SPECIFICATIONS
3820PLATES HSLA ABS SEC 43 NORM * REV-77 GR EH32 +35 CVHT FREQ P 25 FT-LBS -40F.

INSPECTION

ITEM	MATERIAL DESCRIPTION	ONTY	WEIGHT	HEAT NO	PIECE NUMBER	YIELD PSI	TENSILE PSI	% ELONG	% REDUCT	BEND	1	2	3	AVG
001	172 36 X 48													
	BOTH THE FOLLOWING PLATES AND TEST COUPONS WERE NORMALIZED AT 1650 DEGS F FOR 1(MINUTES AND AIR COOLE			49680		58100	74200	27.0-8"						
		4		49680	P58304		TYPE A IMPACT T @			-40 DEGS F FULL SIZE				
										EOY	86	110	113	103
	4 PLATES													

HEAT NUMBER	TYPE	G.S	C	Mn	P	S	Si	Cr	Ni	Mo	Cu	Ti	V	B	Cb	Al	N
49680	LDL	9	12	1.50	.010	.006	21	07	2"	05	20		.001		.001	.032	

FORM 1538 REV 2/78

TABLE 3. MILL REPORT FOR HY80

LUKENS STEEL

TEST CERTIFICATE

Lukens Steel Company
Quality Assurance Laboratory
Coatesville, PA 19320

PAGE NO. 31 OF 32
FILE NO: 0665-01-01
DATE: 02/28/85
MILL ORDER NO: 69521-001

CUSTOMER P.O.: 61466
DESCRIPTION: 1 - 1/2 -W- 60 -E- 210 RECTANGLE

SOLD TO:
BATTELLE MEMORIAL INST.
505 KING AVENUE
COLUMBUS OH 43201

SEND TO: 03-C
BATTELLE MEMORIAL INST.
505 KING AVENUE
ATTN:MR.JOHN F.CLARK
COLUMBUS OH 43201

SHIP TO:
BATTELLE MEMORIAL INST.
505 KING AVENUE
COLUMBUS OH 43201

MIL S-16216J-4A01 VR 82 HY80-TY.I

MELT SLAB 07677 /1JA

CHEMICAL ANALYSIS

	C	MN	P	S	CU	SI	NI	CR	MO	V	TI	B	SA	AS	SN	PRACTICES
07677	.15	.28	.011	.016	.12	.24	2.02	1.02	.24	.006	.005		.0053	.0050	.006	VEP FGP E/P QUALITY
PROD ANALYSIS	.16	.27	.010	.015	.12	.25	2.00	1.05	.25	.004	.003		.0040	.0040	.005	
PROD ANALYSIS	.15	.26	.010	.015	.12	.25	2.05	1.00	.22	.003	.003		.0040	.0050	.005	

TENSILES

TYPE	YIELD PSI X 100	TENSILE PSI X 100	% ELONG IN 2	% R.A.
TX	848	1067	22.0	
LX	871	1061	21.0	

CHARPY V IMPACTS FULL

TYPE	TEMP	FT LBS			MILS LATERAL EXPANSION			% SHEAR		
TX	0	71	76	69						
LX	0	76	73	93						
TX	0	76	80	70						
LX	0	100	89	90						
TX	-120	91	62	56						
TX	-140	65	65	72						

OTHER TESTS PERFORMED

BRINELL - 214 248 PLATE

INFORMATION

WEIGHT PER PIECE = 1797
ALL TEMPERATURES APPEAR IN DEGREES FAHRENHEIT.
PRODUCED IN ACCORDANCE WITH INSPECTION SYSTEM
--REQUIREMENTS OF MIL-I-45208A
NDE, VISUAL AND DIMENSIONAL INSPECTION AS REQUIRED BY THE SPECIFICATION WAS SATISFACTORILY PERFORMED.
MATERIAL HAS BEEN SAMPLED, TESTED, AND INSPECTED IN ACCORDANCE WITH THE SPECIFICATION REQUIREMENTS. THE MANUFACTURER HAS MAINTAINED MANUFACTURING PROCEDURES AND PRACTICES WHICH PRODUCE PLATES WHICH MEET THE MINIMUM PROPERTY REQUIREMENTS THROUGHOUT THE PLATE. THE MATERIAL MEETS ALL SPECIFICATION REQUIREMENTS.

HEAT TREAT CYCLES MATL OR TESTS DEG F

MATL	TEST	NOM TEMP	MIN TEMP	MAX TEMP	HOLD MINS	COOL METHOD	END TEMP
K	K	1660			0001	WQ	
K	4	1300			0001	AC	

HEAT TREAT CYCLES TESTS ONLY DEG F

START END TEMP	NOM TEMP	MIN TEMP	MAX TEMP	HOLD MINS	HEAT RATE MAX	COOL RATE MAX

LUKENS STEEL

TEST CERTIFICATE

Lukens Steel Company
Quality Assurance Laboratory
Coatesville, PA 19320

PAGE NO. 32 OF 32
FILE NO 0665-01-01
DATE 02/28/85
MILL ORDER NO. 69521-001

CUSTOMER PO 61466
DESCRIPTION 1 - 1/2 -W- 60 -E- 210 RECTANGLE

SOLD TO.
BATTELLE MEMORIAL INST.
505 KING AVENUE
COLUMBUS OH 43201

SEND TO: 03-C
BATTELLE MEMORIAL INST.
505 KING AVENUE
ATTN:MR.JOHN F.CLARK
COLUMBUS OH 43201

SHIP TO:
BATTELLE MEMORIAL INST.
505 KING AVENUE
COLUMBUS OH 43201

MIL S-16216J-4A01 VR 82 HY80-TY.I

MELT SLAB 07677 /1JA

CHEMICAL ANALYSIS

	C	MN	P	S	CU	SI	NI	CR	MO	V	TI	B	PRACTICES
07677 /1JA													

TENSILES

TYPE	YIELD PSI X 100	TENSILE PSI X 100	% ELONG IN	% R.A.

CHARPY V IMPACTS FULL

TYPE	TEMP	FT LBS			MILS LATERAL EXPANSION			% SHEAR		
RX	-120	130	113	113						
LX	-120	78	73	82						

OTHER TESTS PERFORMED

INFORMATION

RECORDS ARE AVAILABLE COVERING HEAT NUMBER OF THE MATERIAL USED, PROCESSING OF PLATE, DIMENSIONAL CONTROL EMPLOYED AND HEAT TREATMENT.
92755 L22465.

HEAT TREAT CYCLES MATL OR TESTS DEG F

MATL	TEST	NOM TEMP	MIN TEMP	MAX TEMP	HOLD MINS	COOL METHOD	END TEMP

HEAT TREAT CYCLES TESTS ONLY DEG F

START END TEMP	NOM TEMP	MIN TEMP	MAX TEMP	HOLD MINS	HEAT RATE MAX	COOL RATE MAX

WE HEREBY CERTIFY THE ABOVE INFORMATION IS CORRECT:

R. R. Romanchik
SUPERVISOR TEST REPORTING

TABLE 4. RESULTS OF FRACTURE-TOUGHNESS TESTS

Steel	Specimen(a)	Type of Precrack(b)	J_{Ic}		K_{Jc} (= EJ_{Ic})$^{1/2}$	
			kJ/m^2	lb/in.	MPa$\sqrt{m}$	ksi$\sqrt{in.}$
EH36	EH-2	E813	139.8	800	170.1	154.7
	EH-5	E813	142.3	814	171.6	156.0
	EH-3	OL	150.1	863	176.7	160.6
	EH-4	OL	154.8	886	179.0	162.8
	EHPD-1	E813	137.4	786	168.6	153.3
	EHPD-2	E813	147.3	843	174.6	158.8
HY80	HY-1	E813	271.7	1555	237.2	215.6
	HY-2	E813	265.4	1519	234.4	213.1
	HY-3	OL	305.8	1750	251.6	228.7
	HY-4	OL	315.6	1806	255.6	232.4
	HYPD-1	E813	265.4	1519	234.4	213.1
	HYPD-2	E813	307.4	1759	252.3	229.3

(a) PD indicates that the material was predamaged by fatigue cycling before the specimen was fabricated.

(b) E813 indicates precracking in accordance with ASTM E813 and OL indicates precracking at about 0.6 times limit load.

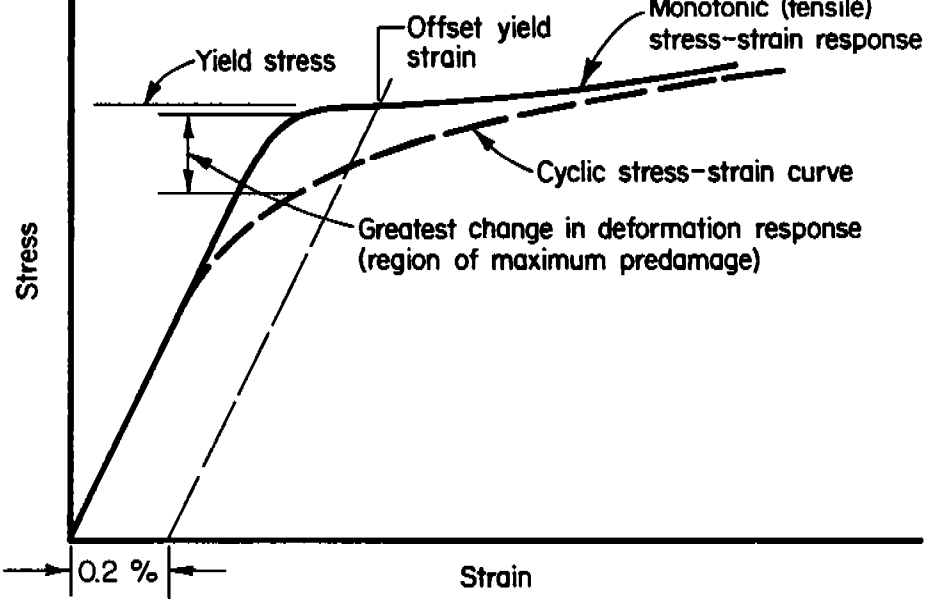

FIGURE 1. SCHEMATIC DEFINING DAMAGE AND INDICATING THE REGION OF MAXIMUM PREDAMAGE.

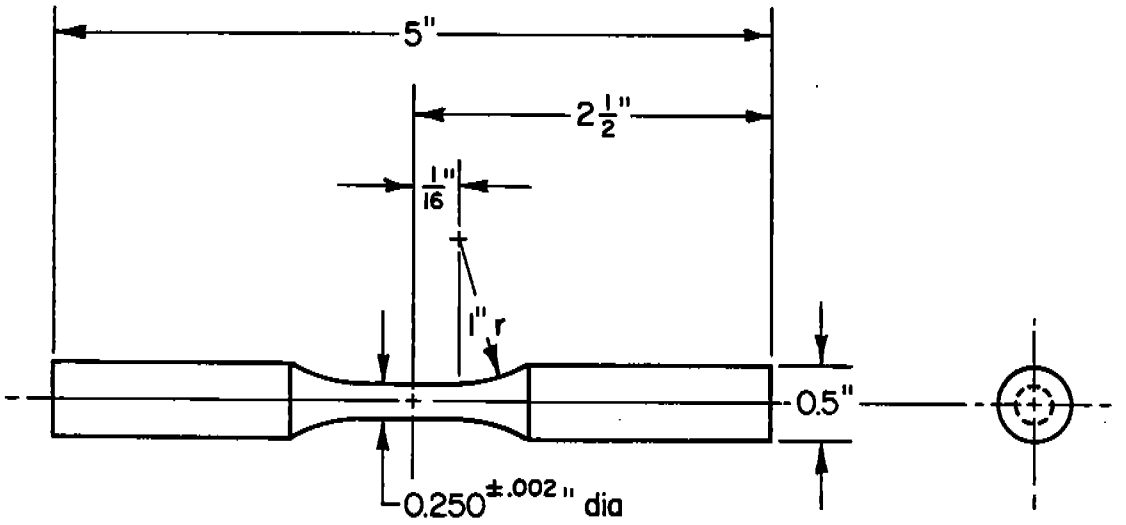

FIGURE 2. AXIAL SMOOTH SPECIMEN FOR DEFORMATION RESPONSE STUDIES.

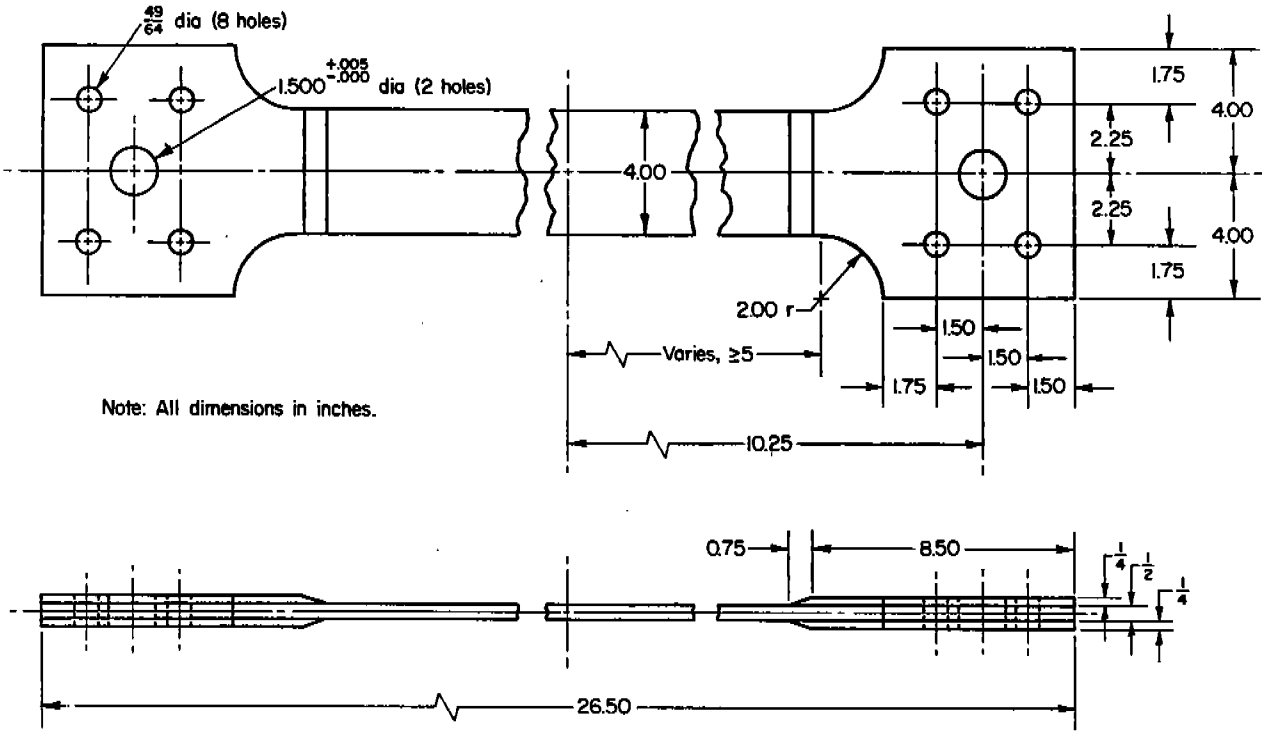

FIGURE 3. PREDAMAGE PANELS USED TO DEVELOP BULK PREDAMAGE: USED IN CONJUNCTION WITH BUCKLING RESTRAINTS.

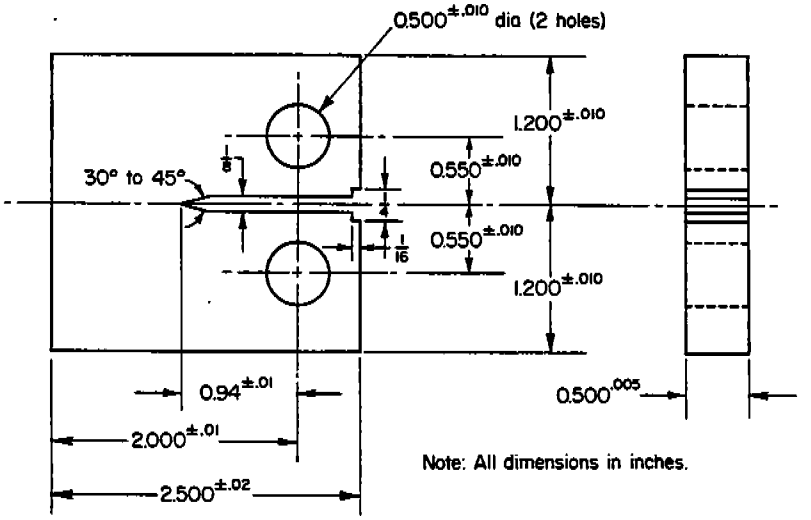

FIGURE 4. J-TOUGHNESS SPECIMEN.

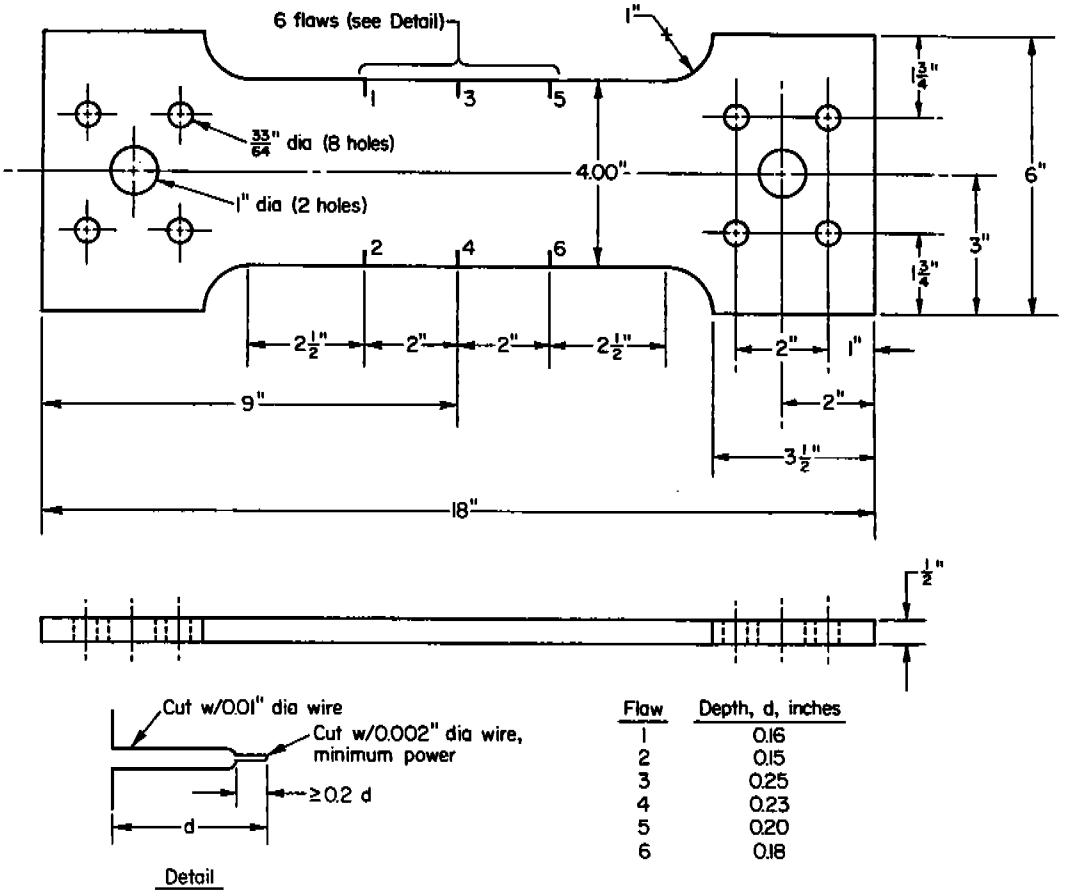

Flaw	Depth, d, inches
1	0.16
2	0.15
3	0.25
4	0.23
5	0.20
6	0.18

FIGURE 5. MULTI-FLAW CRACK GROWTH SPECIMEN.

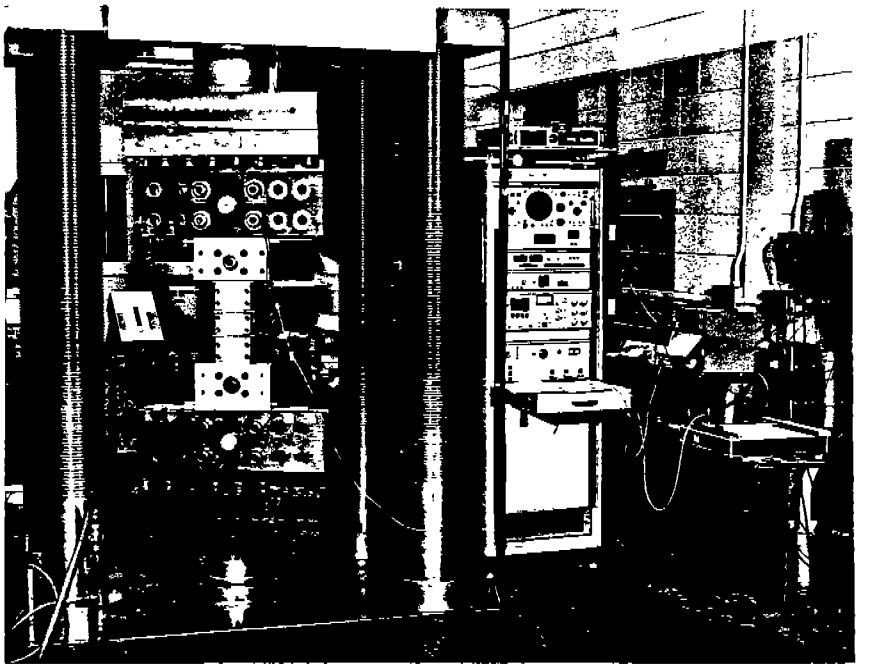

-3/4 7484

FIGURE 6. PHOTOGRAPH OF SET UP TO IMPOSE BULK PREDAMAGE.

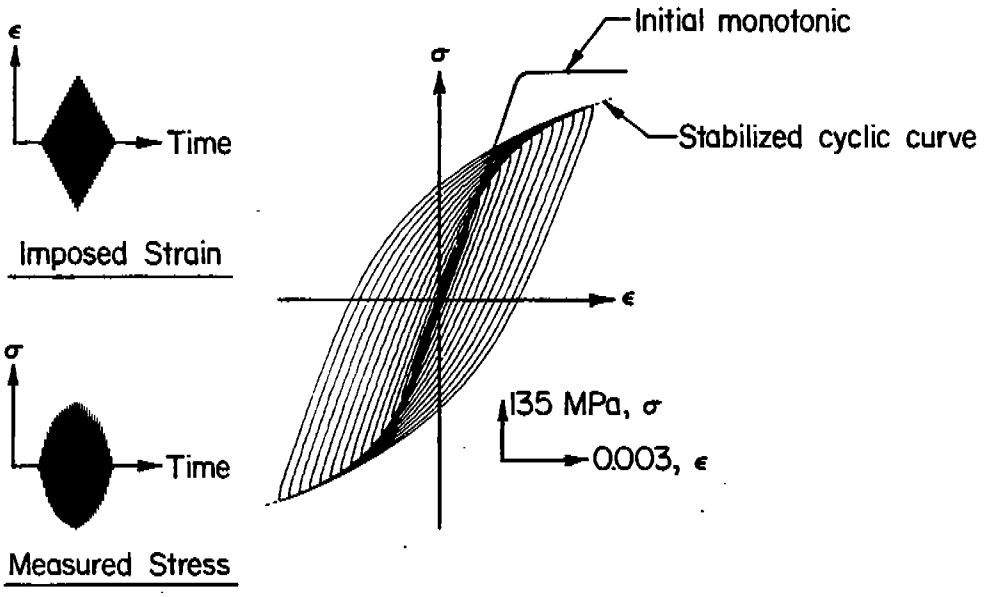

FIGURE 7. FORCING FUNCTION, AND RESPONSE AS MEASURED STRESS AND AS STRESS-STRAIN BEHAVIOR.

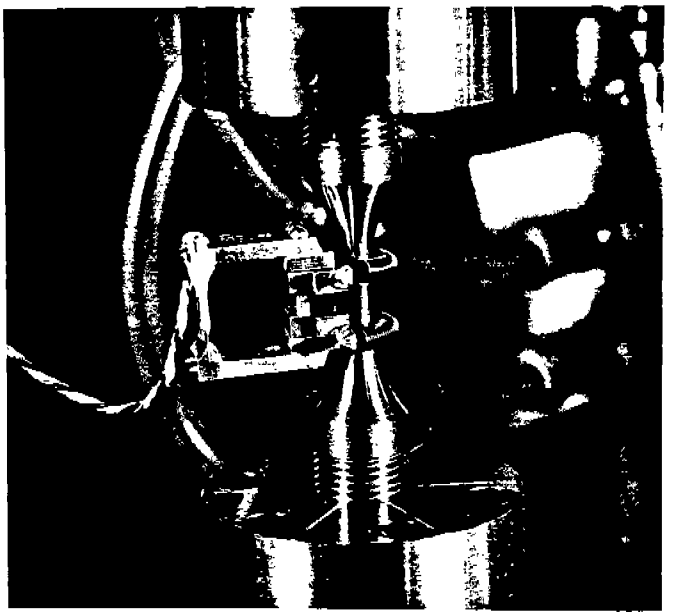

C-9472

FIGURE 8. SET-UP FOR INCREMENTAL STEP TEST.

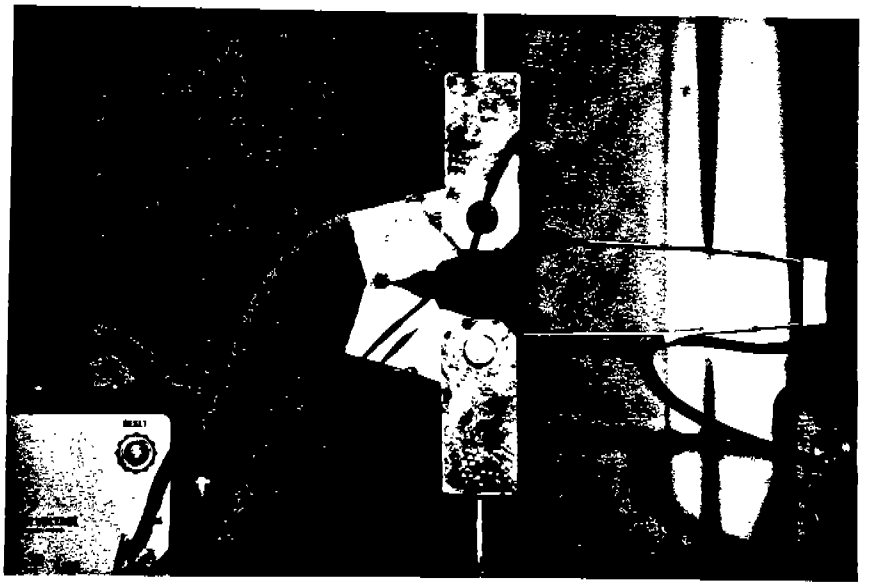

FIGURE 9. TYPICAL TEST SET UP FOR SINGLE SPECIMEN J_{IC} CURVE TOUGHNESS MEASUREMENT (NEAR TERMINATION).

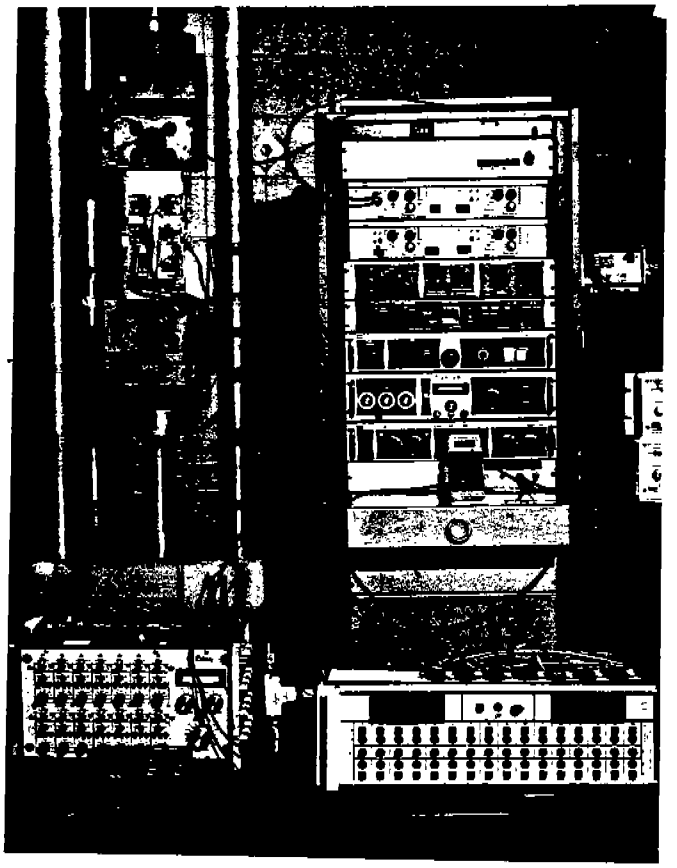

-1/2 7485

FIGURE 10. FATIGUE CRACK GROWTH TEST SET UP.

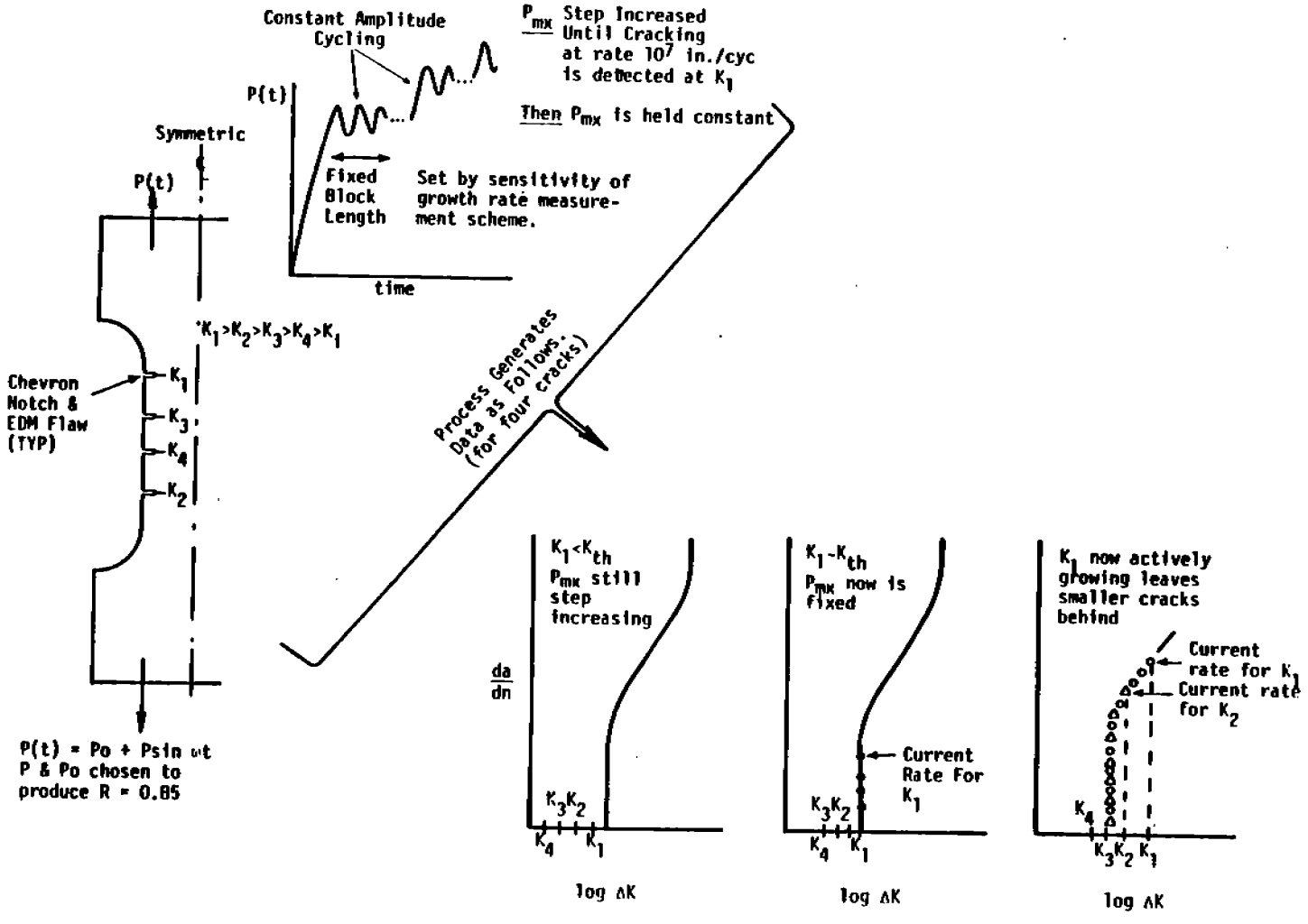

FIGURE 11. SCHEMATIC OF THE MULTI-FLAW INCREMENTAL LOAD STEP THRESHOLD TEST METHOD.

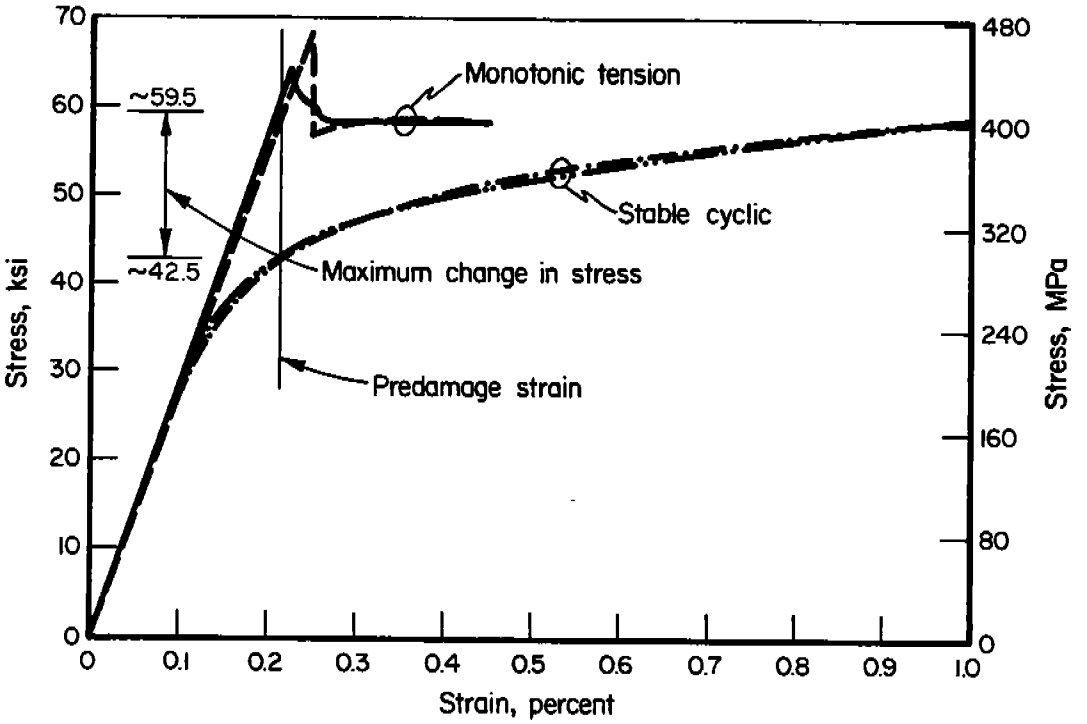

a. EH36.

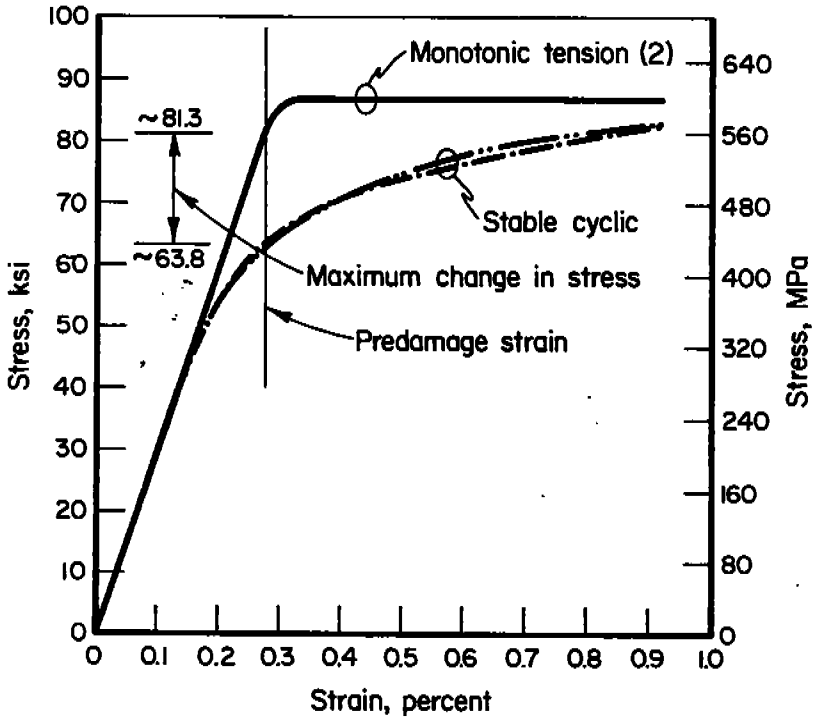

b. HY80.

FIGURE 12. MONOTONIC AND CYCLIC DEFORMATION RESPONSE FOR EH36 AND HY80 STEELS.

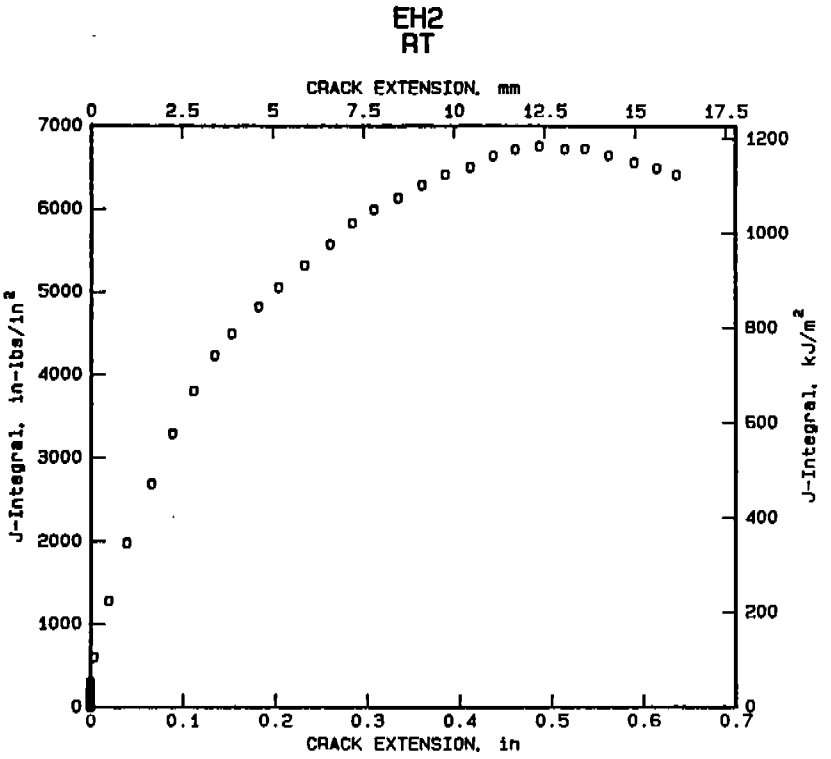

a. EH2: E813 precrack in virgin EH36.

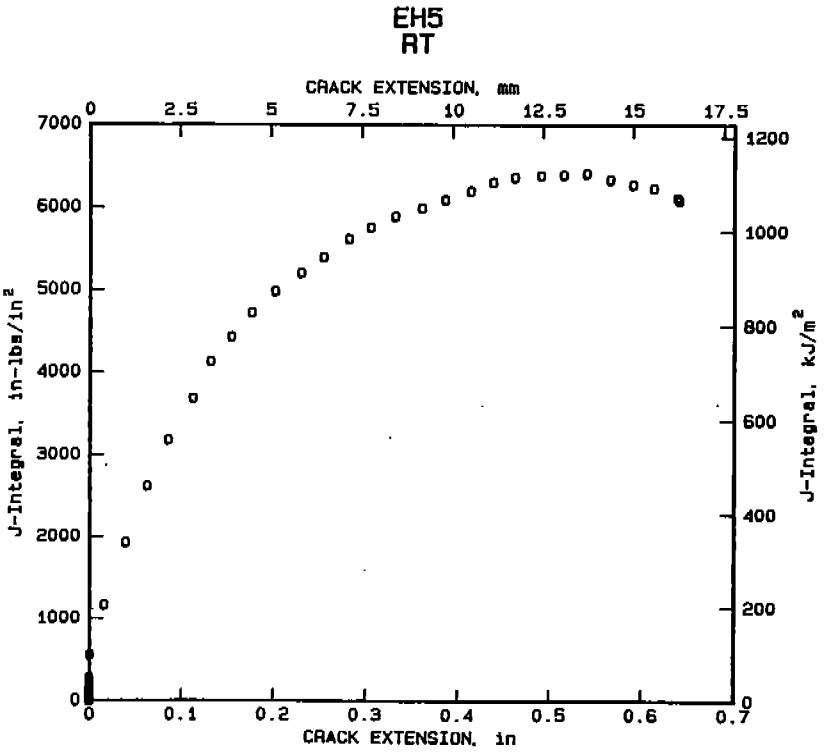

b. EH5: E813 precrack in virgin EH36 (duplicate of (a)).

FIGURE 13. J-R CURVES FOR EH36 STEEL.

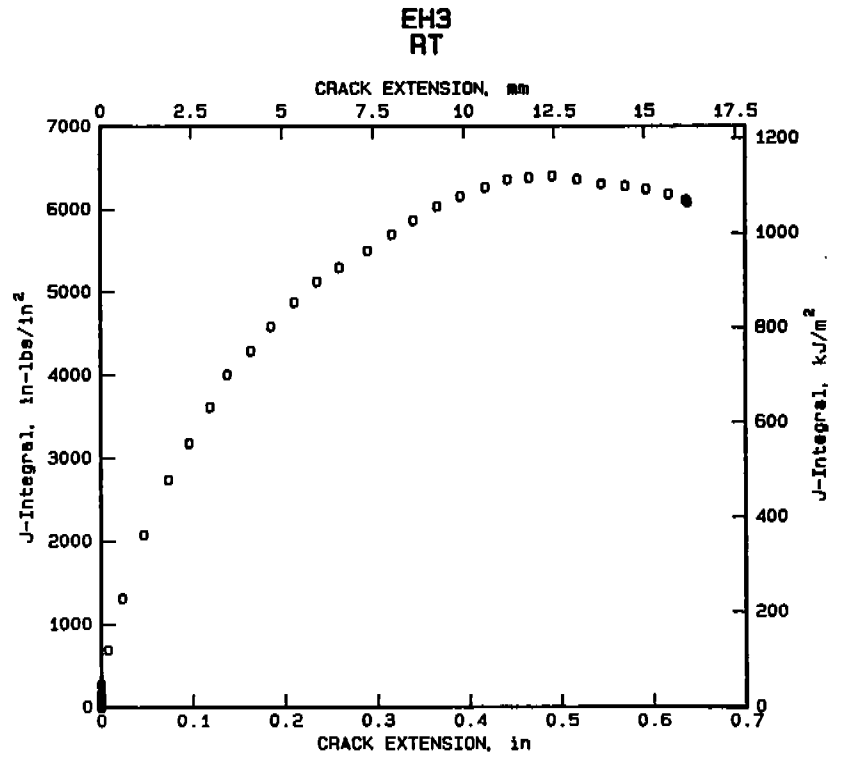

c. EH3: 0.6 x limit load precrack in virgin EH36.

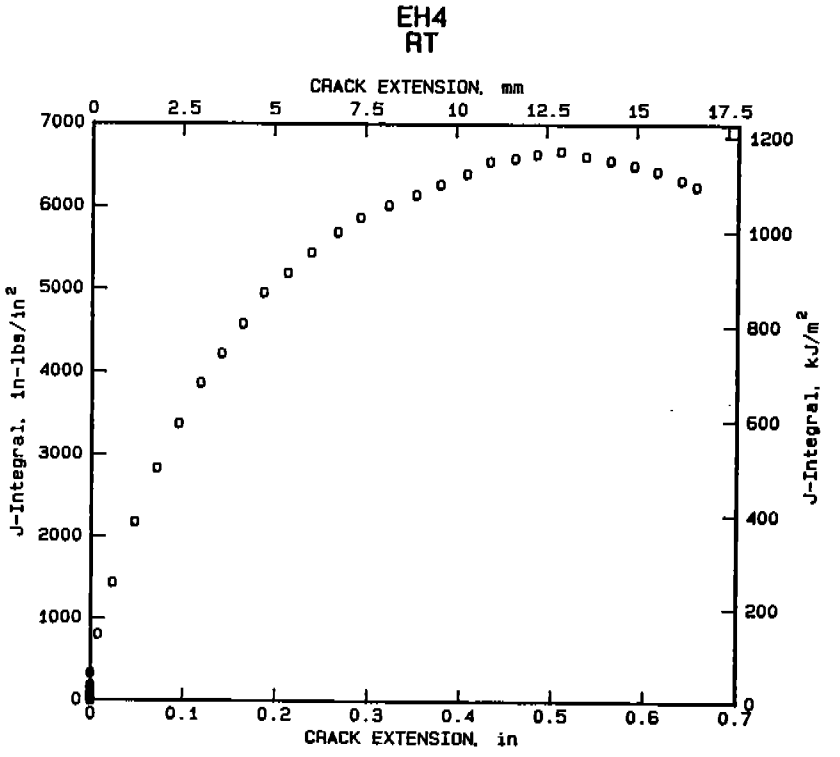

d. EH4: 0.6 x limit load precrack in virgin EH36 (duplicate of (c)).

FIGURE 13. (Continued).

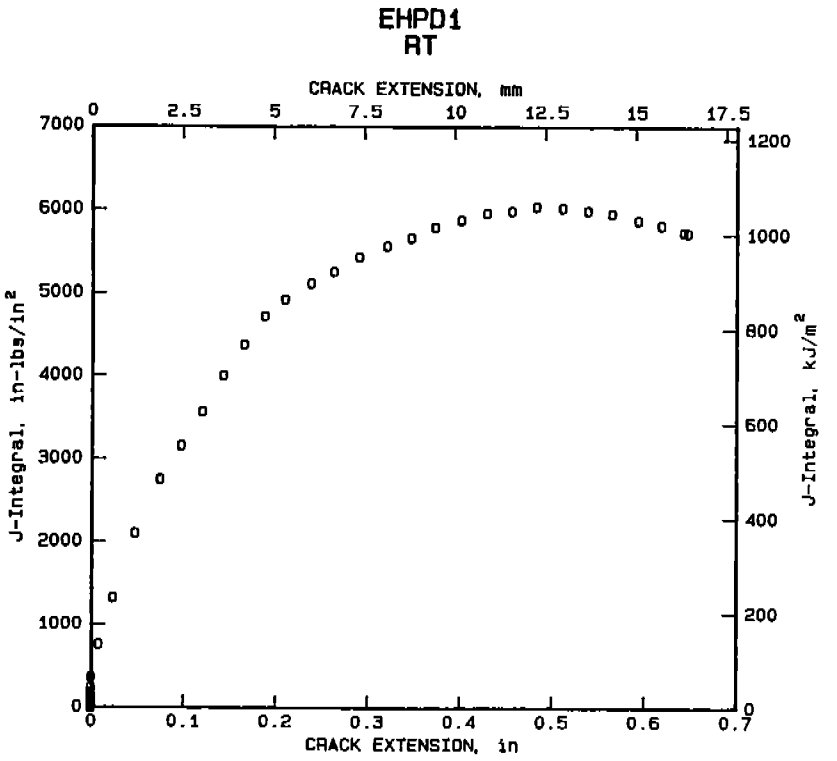

e. EHPD1: E813 precrack in bulk predamaged EH36

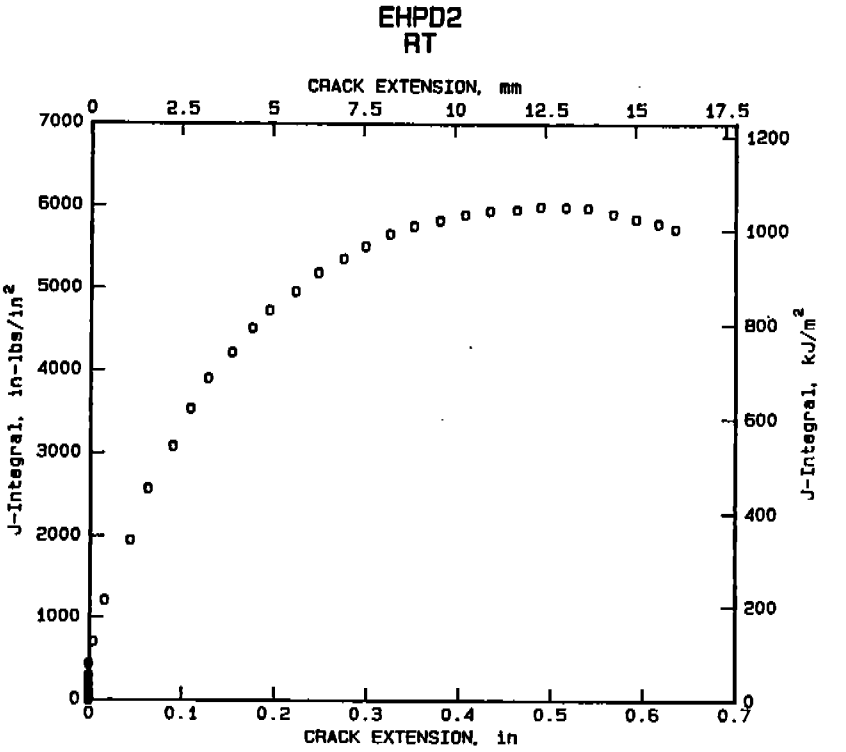

f. EHPD2: E813 precrack in bulk predamaged EH36 (duplicate of (e)).

FIGURE 13. (Concluded).

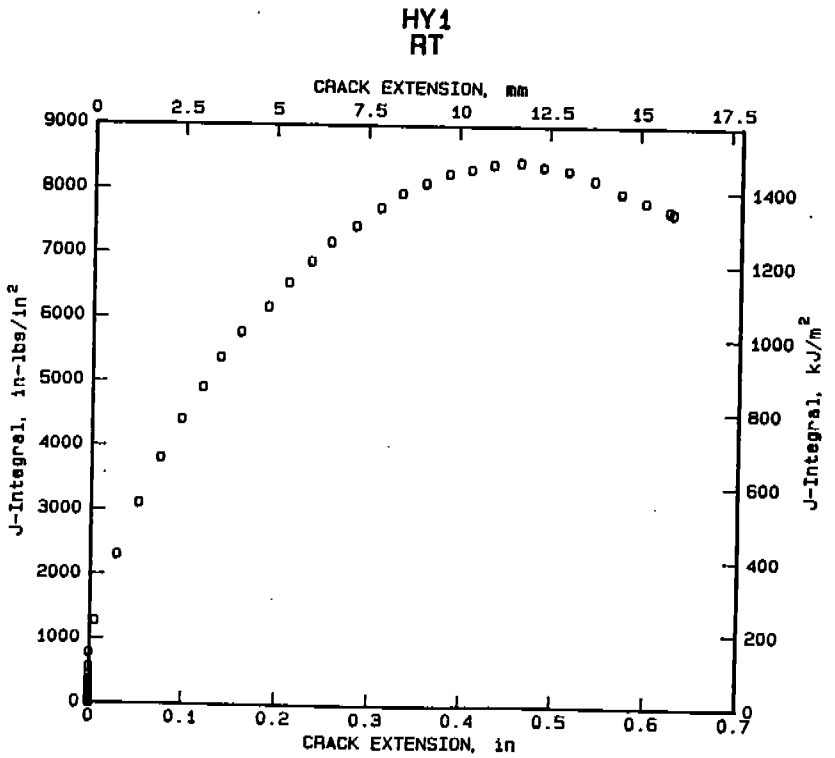

a. HY1: E813 precrack in virgin HY80.

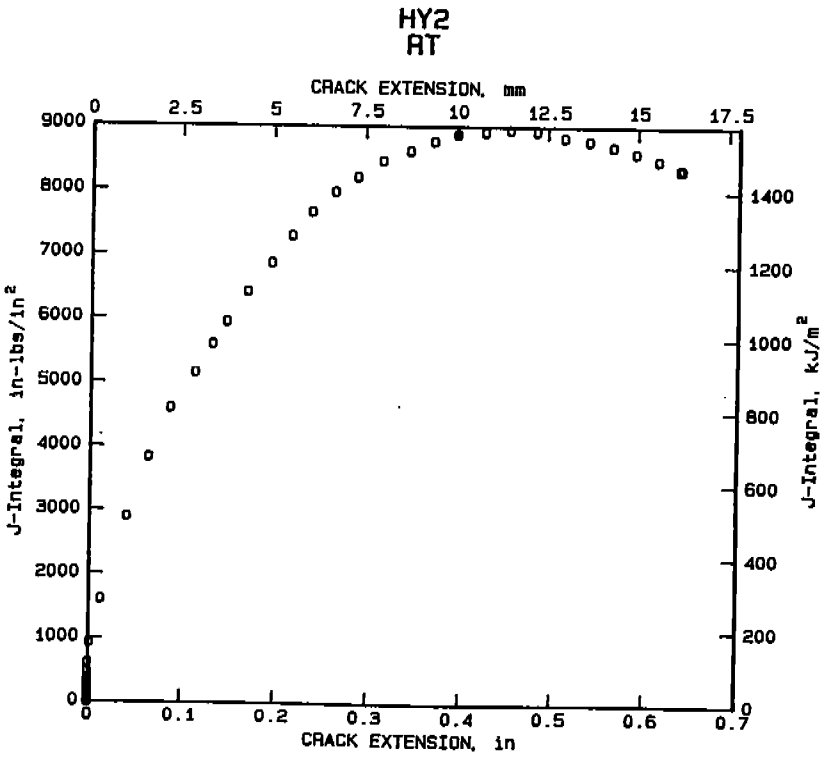

b. HY2: E813 precrack in virgin HY80 (duplicate of (a)).

FIGURE 14. J-R CURVES FOR HY80 STEEL.

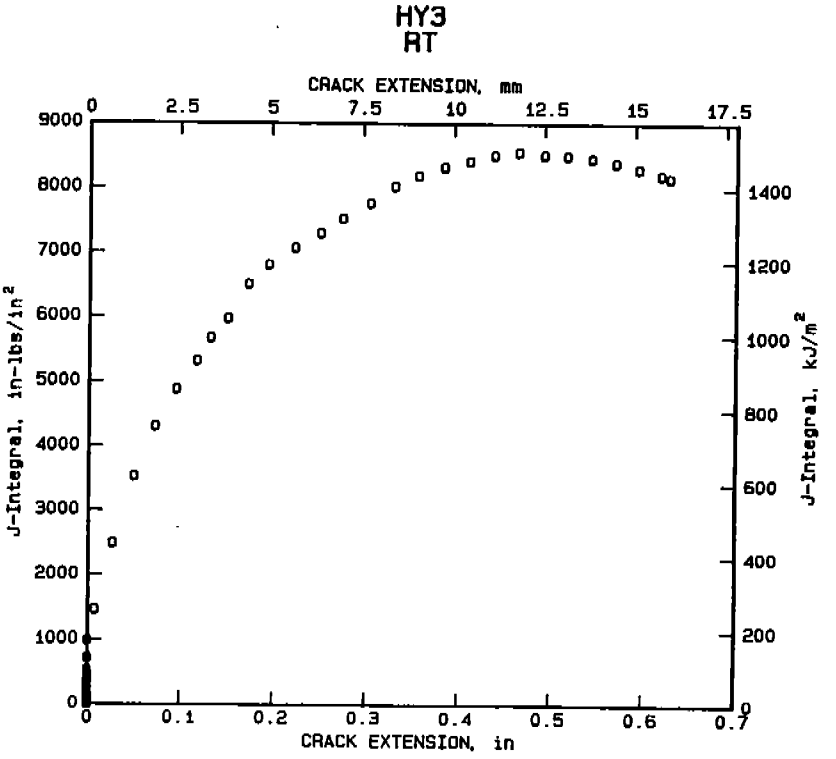

c. HY3: 0.6 x limit load precrack in virgin HY80.

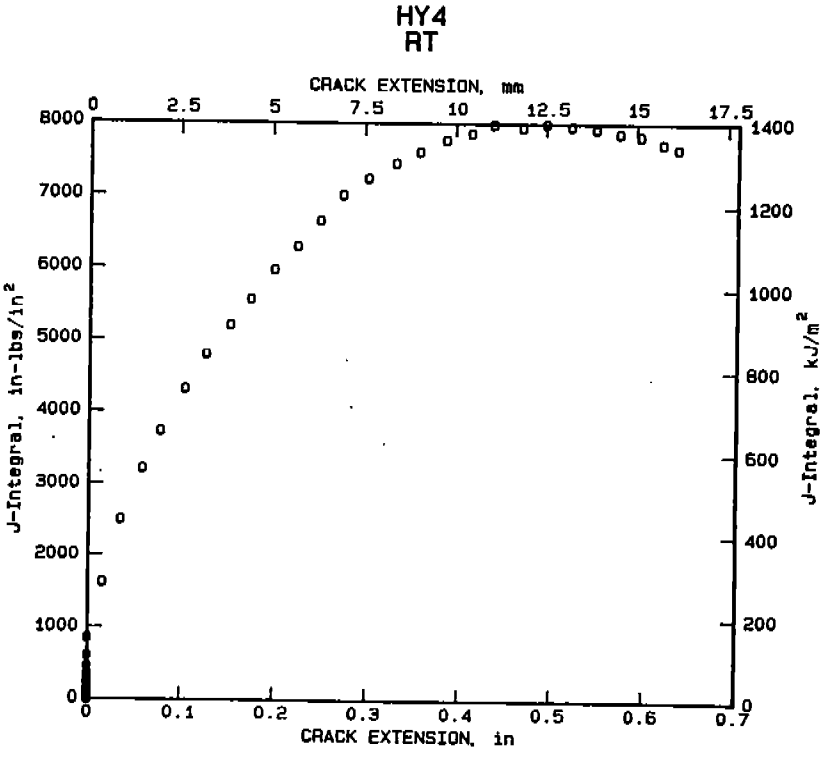

d. HY4: 0.6 x limit load precrack in virgin HY80 (duplicate of (c)).

FIGURE 14. (Continued).

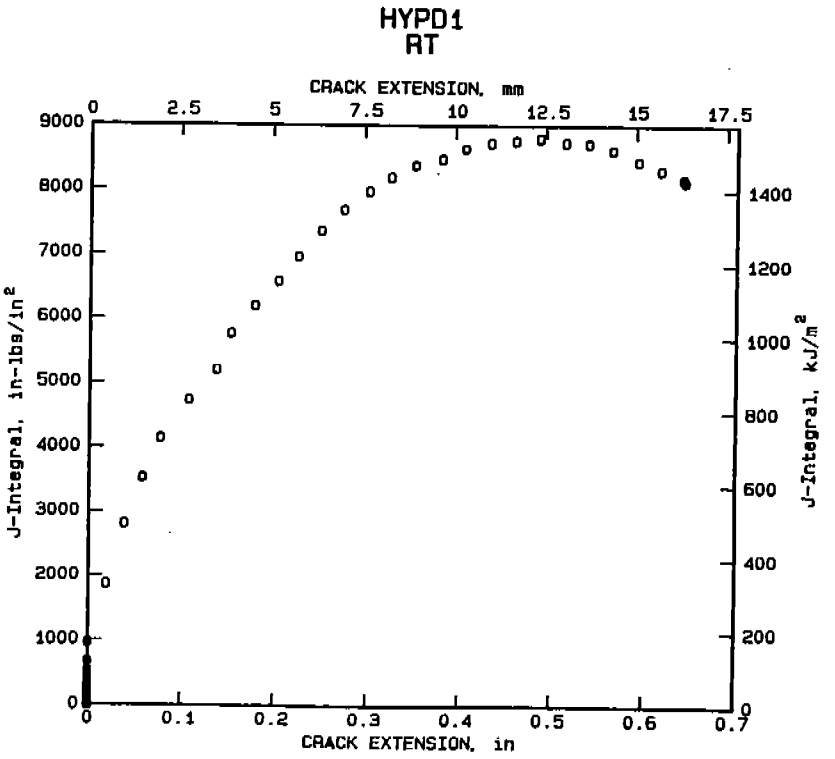

e. HYPD1: E813 precrack in bulk predamaged HY80.

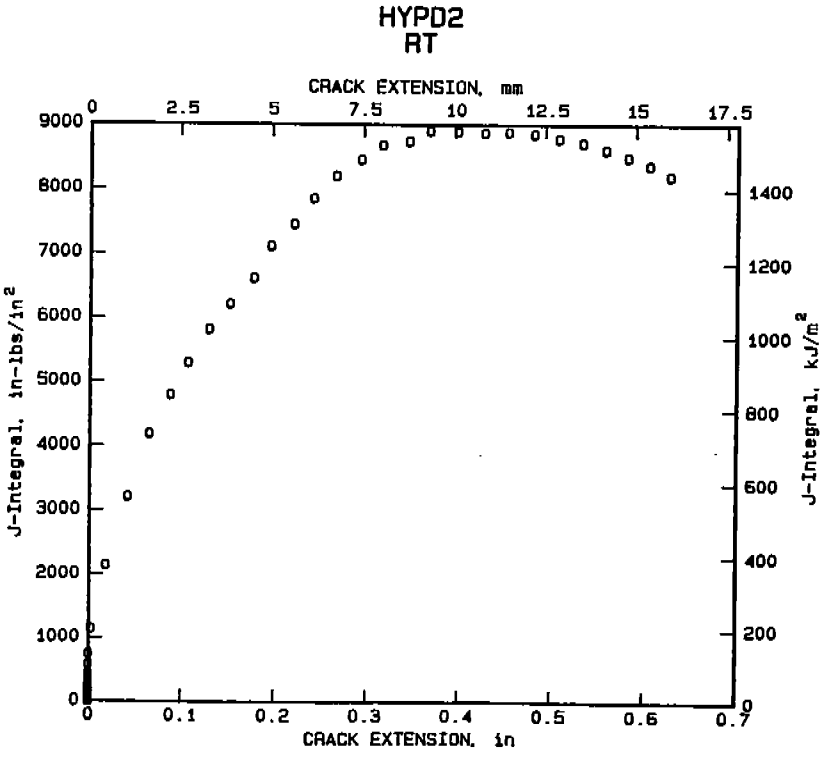

f. HYPD2: E813 precrack in bulk predamaged HY80 (duplicate of (e)).

FIGURE 14. (Concluded).

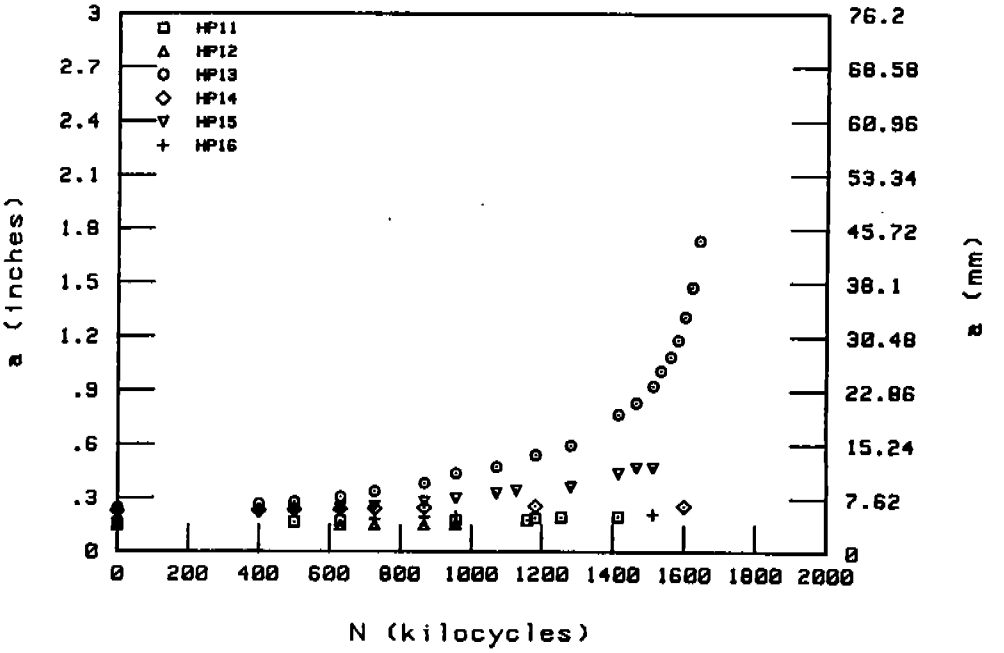

FIGURE 15. CRACK LENGTH VERSUS CYCLES FOR HP1.

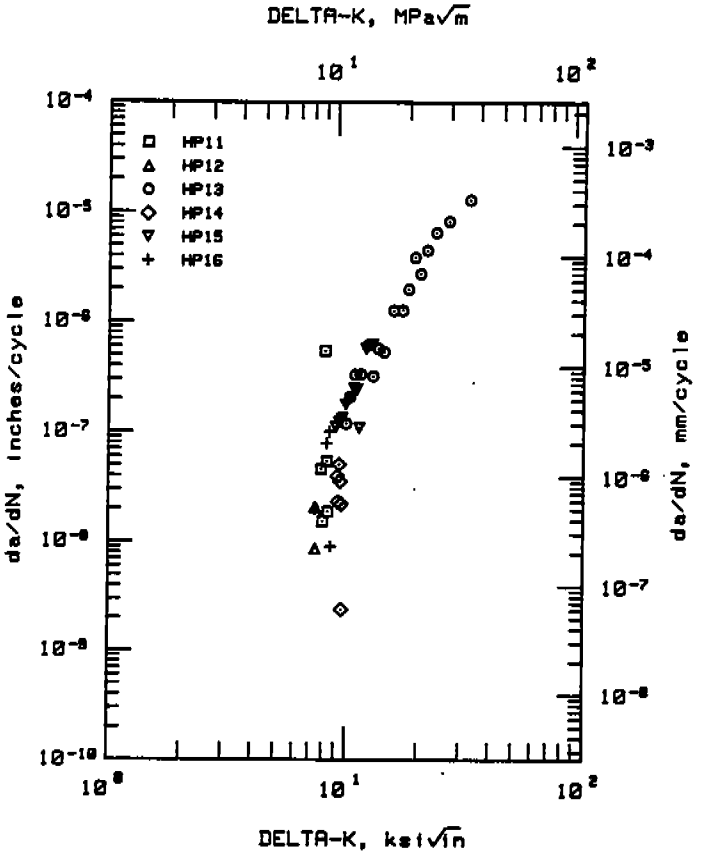

FIGURE 16. da/dN-ΔK BEHAVIOR FOR HP1.

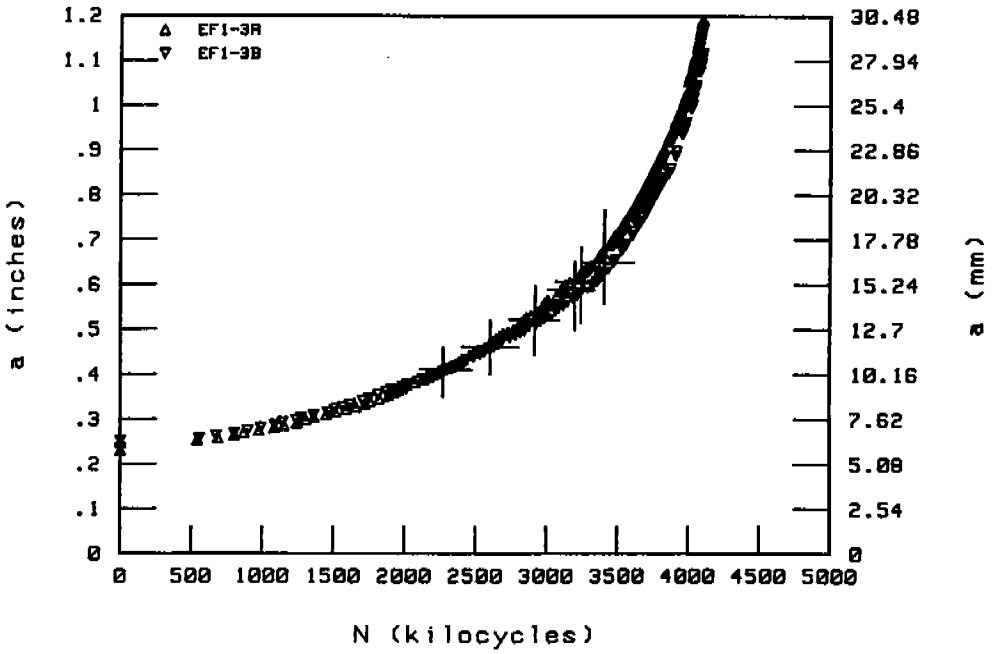

FIGURE 17. CRACK LENGTH VERSUS CYCLES BEHAVIOR FOR EF1, FLAW 3 ILLUSTRATING CONTINUITY IN GROWTH TREND AFTER LOAD STEPS.

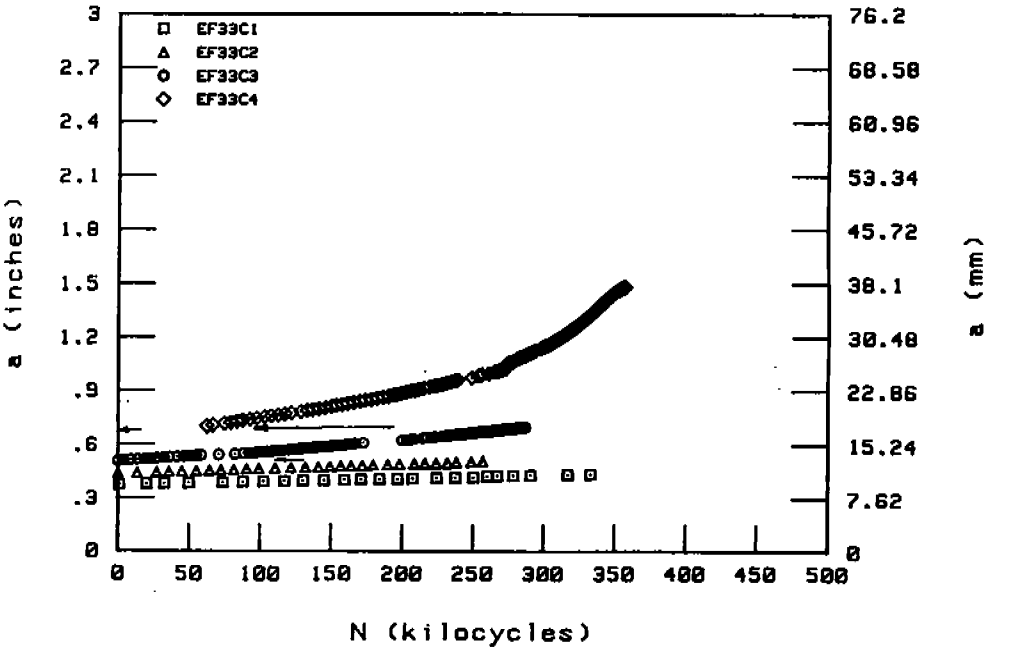

FIGURE 18. CRACK LENGTH VERSUS CYCLES BEHAVIOR FOR EF3, FLAW 3 SHOWING ABSENCE OF TRANSIENTS AT LOAD STEPS IN A SALTWATER ENVIRONMENT.

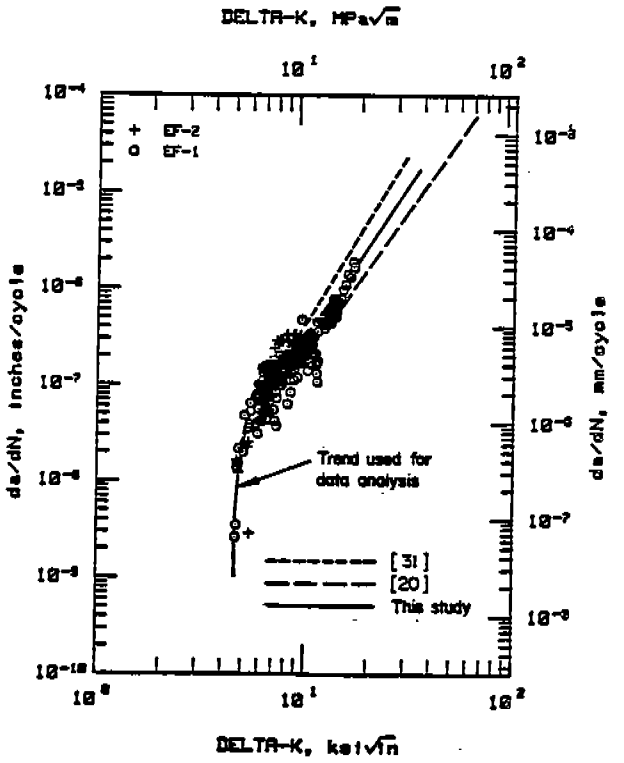

a. As-Received EH36 (EF1 and EF2)

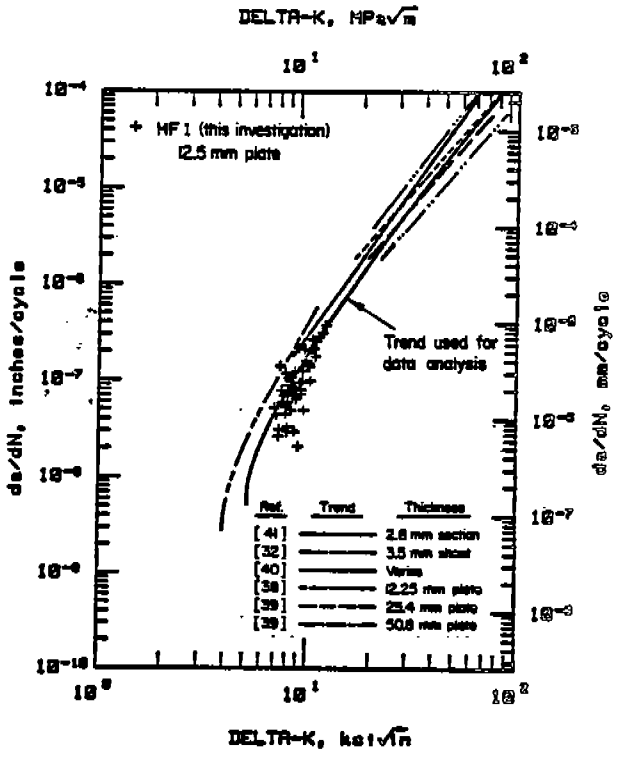

b. As-Received HY80 (HF1)

FIGURE 19. CRACK-GROWTH-RATE VERSUS ΔK FOR VIRGIN AND PREDAMAGED EH36 AND HY80 AT R = 0.01 UNDER AMBIENT CONDITIONS

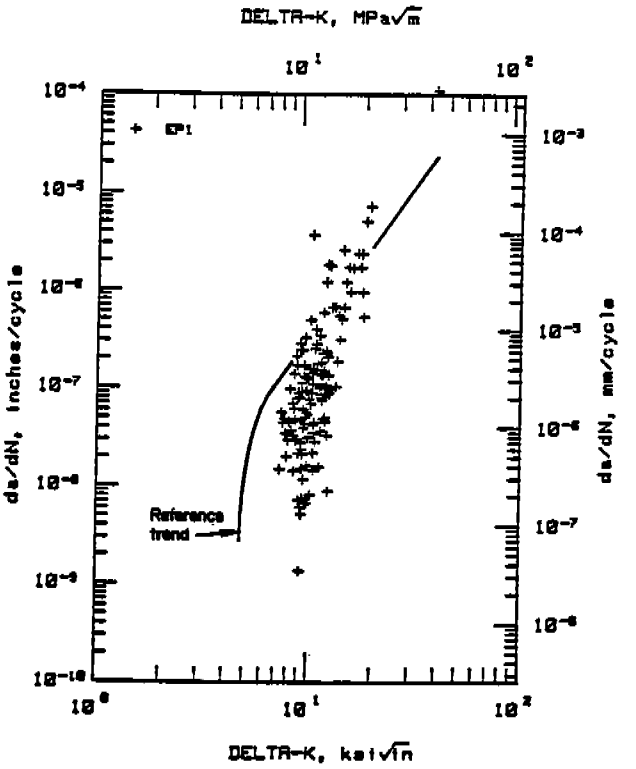

c. Predamaged EH36 (EP1).

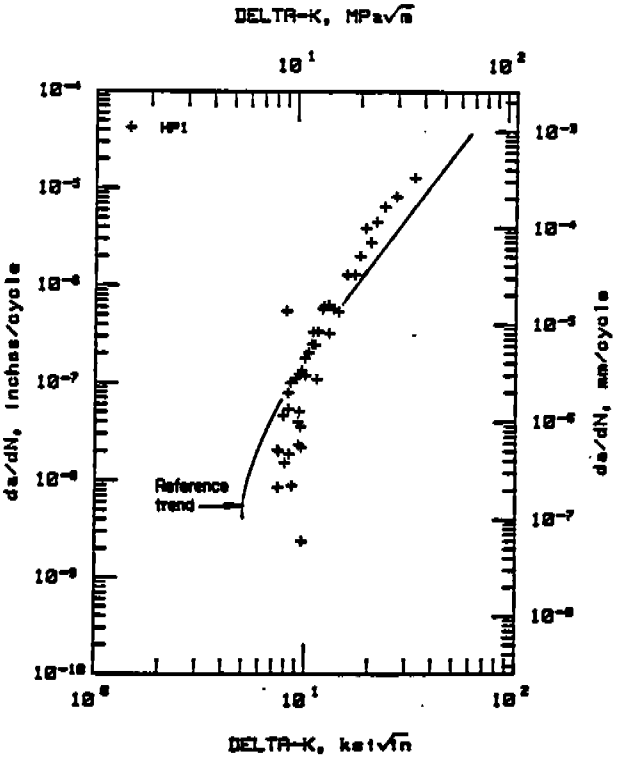

d. Predamaged HY80 (HP1).

FIGURE 19. (Concluded).

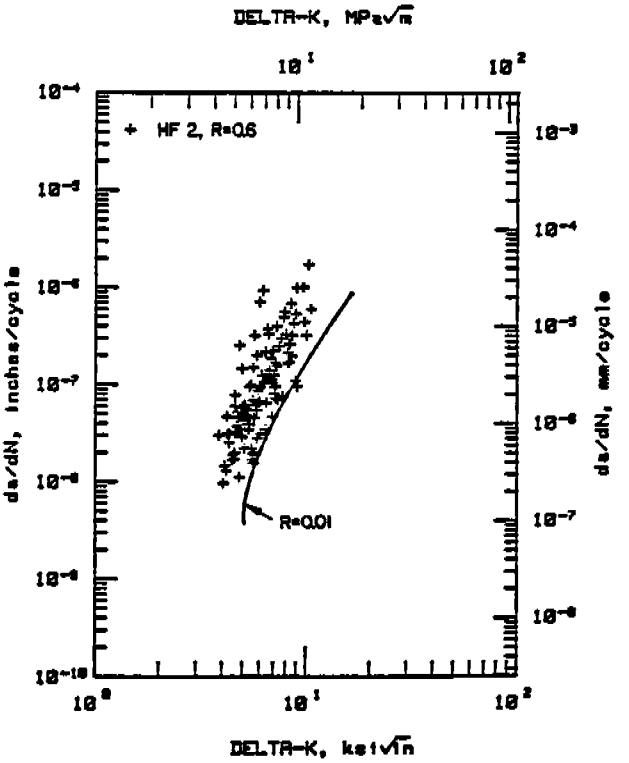

a. HY80: da/dN versus K .

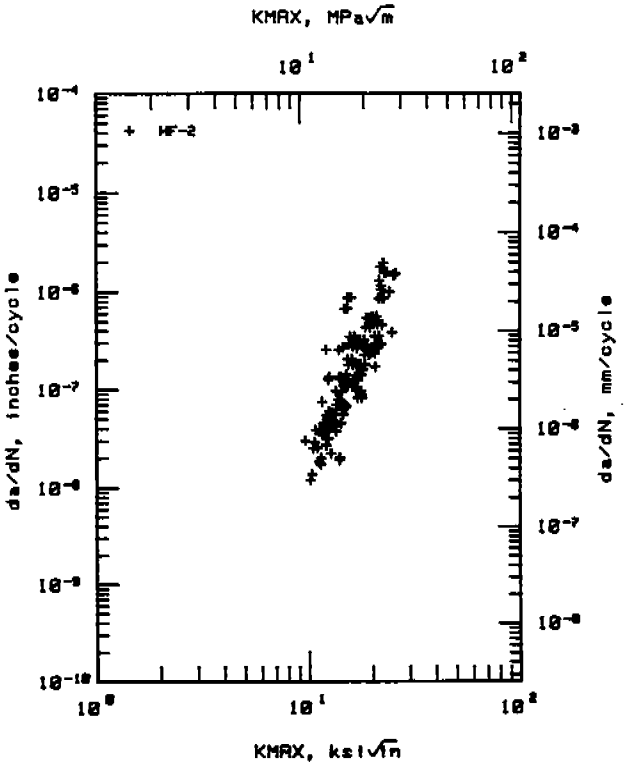

b. HY80: da/dN versus K_{max}.

FIGURE 20. CRACK-GROWTH-RATE VERSUS ΔK FOR REFERENCE HY80 AT STRESS RATIOS OF 0.01 AND 0.6 (HF2).

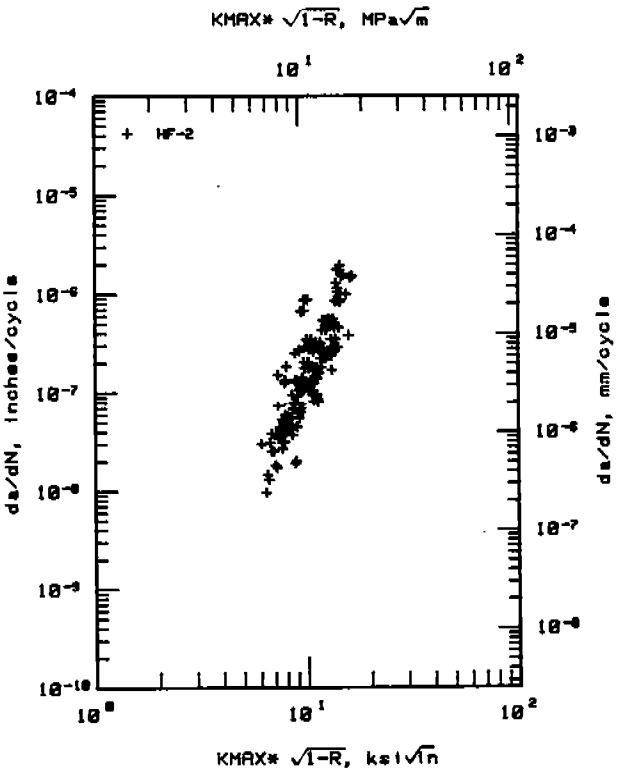

c. HY80: da/dN versus $K_{max}\sqrt{1-R}$[43]

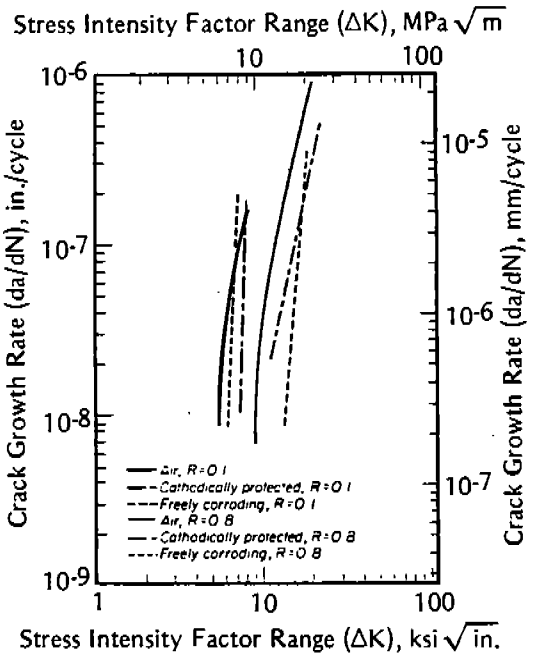

d. Literature data[44]: da/dN versus ΔK

FIGURE 20. (Concluded).

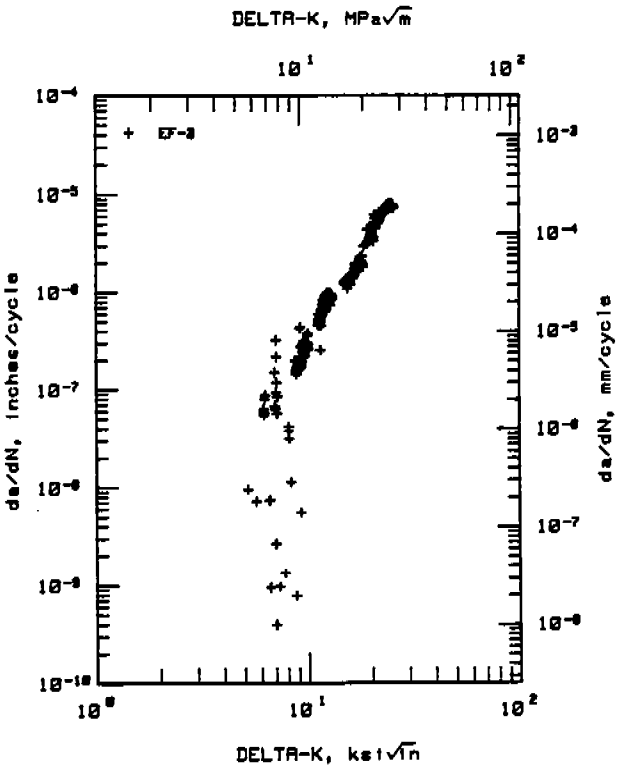

a. Virgin EH36 (EF3).

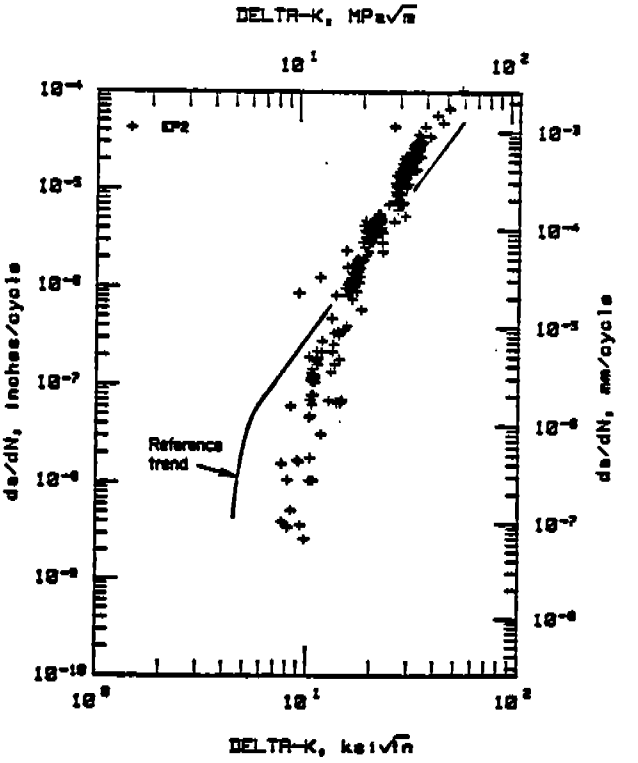

b. Predamaged EH36 (EP2).

FIGURE 21. CRACK-GROWTH-RATE VERSUS ΔK FOR EH36 IN SEAWATER AT R=0.01 AND f=0.5 Hz.

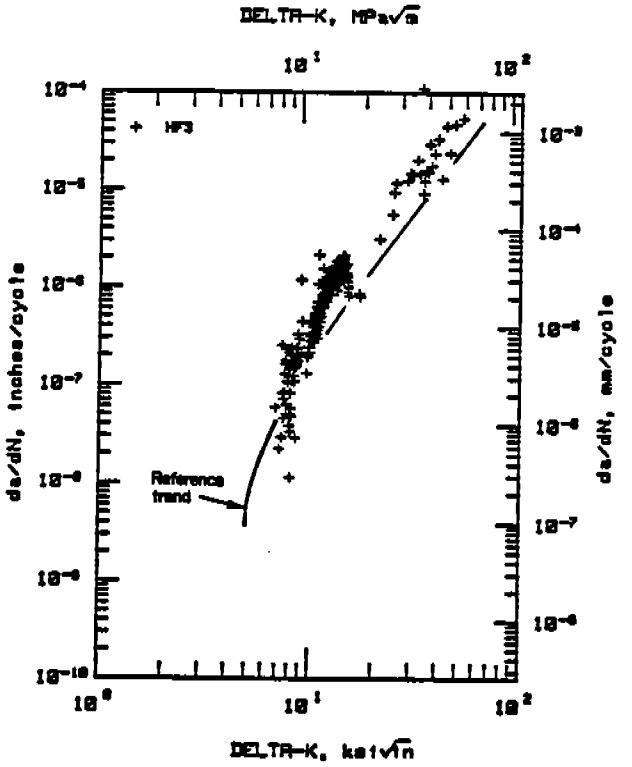

a. Virgin HY80 (HF3); f = 0.5 Hz.

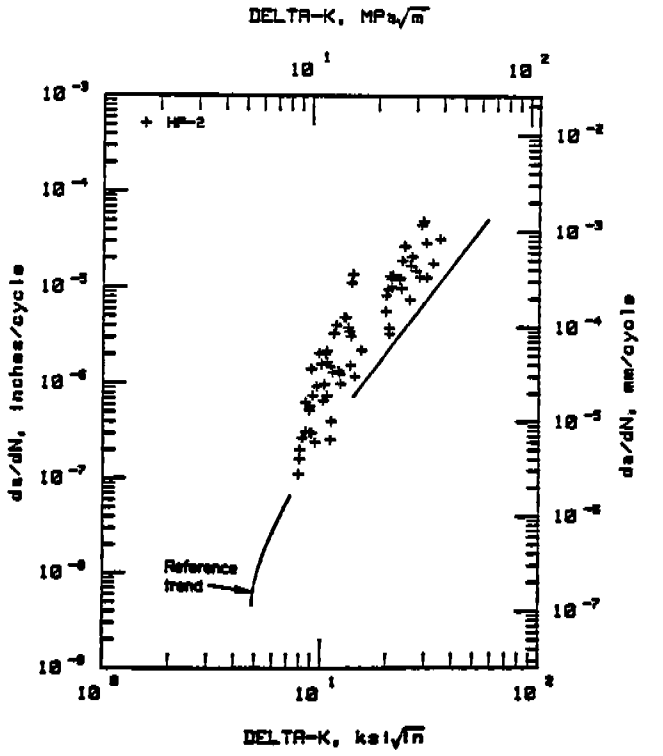

b. Predamaged HY80 (HP2); f = 0.5 Hz.

FIGURE 22. CRACK-GROWTH-RATE VERSUS ΔK FOR HY80 IN SEAWATER AT R = 0.01.

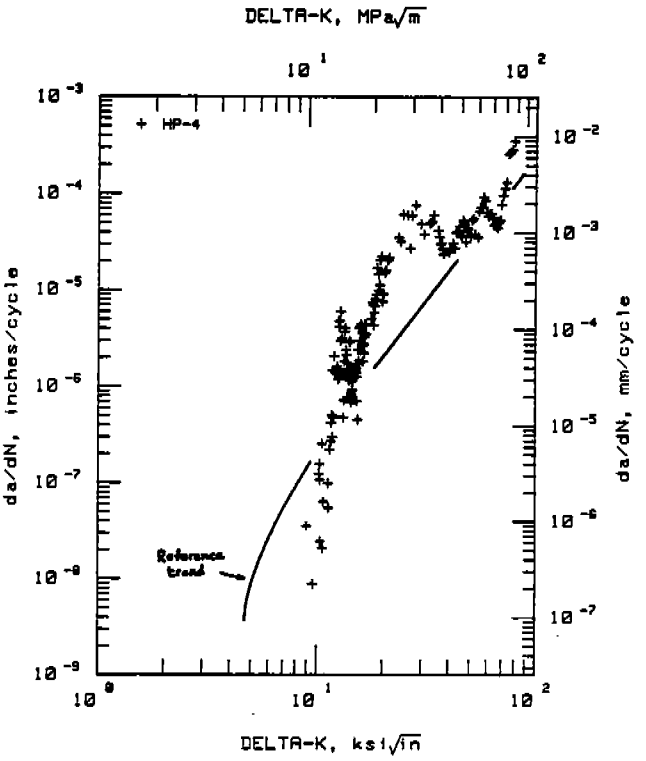

c. Predamaged HY80 (HP4); f = 0.2 Hz.

FIGURE 22. (Concluded).

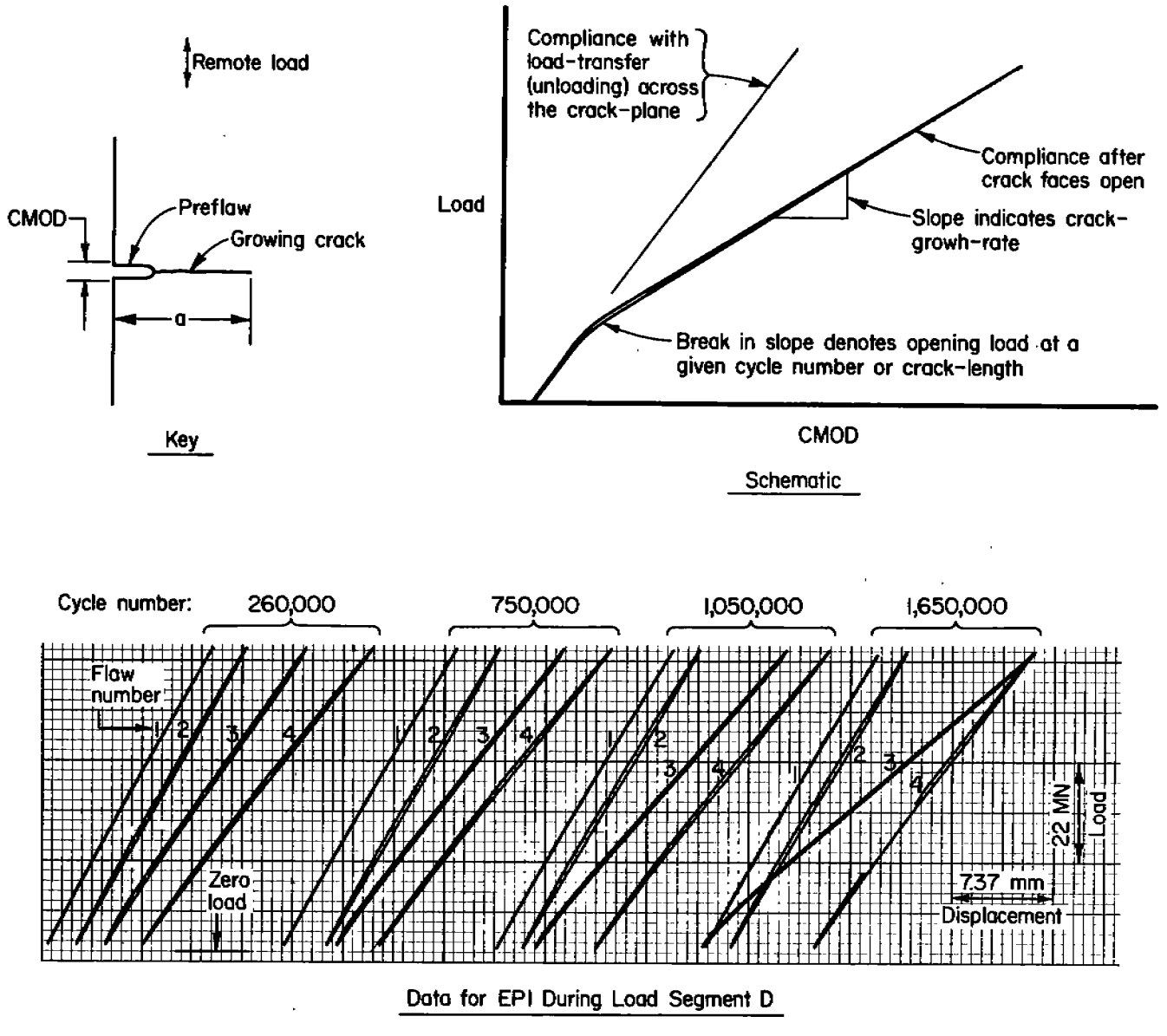

FIGURE 23. TYPICAL LOAD-CMOD BEHAVIOR ILLUSTRATING CLOSURE.

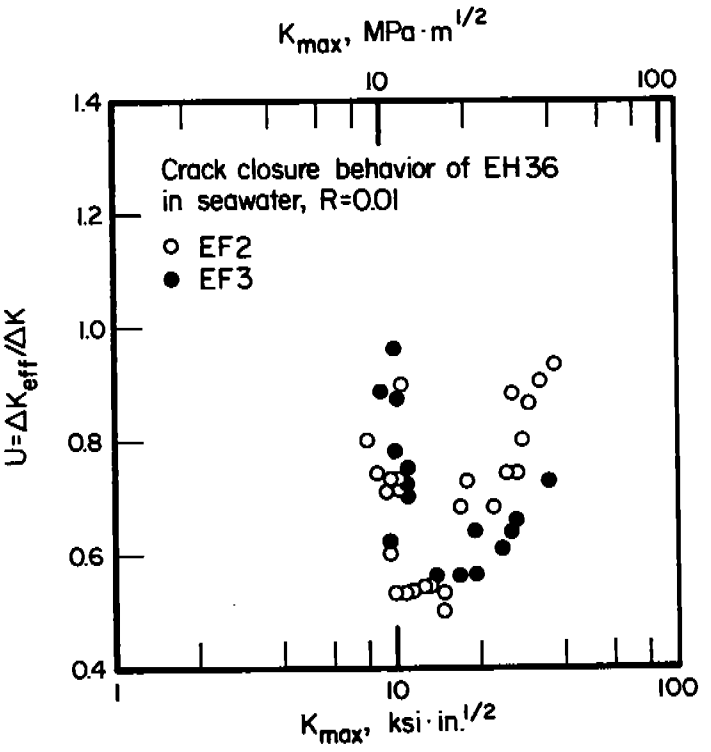

a. EH36.

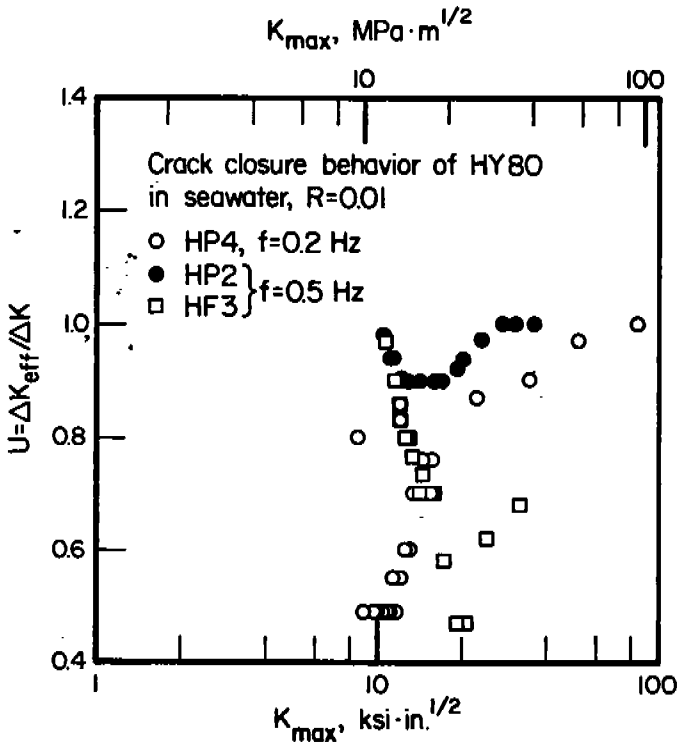

b. HY80.

FIGURE 24. CLOSURE BEHAVIOR DEVELOPED FROM LOAD-CMOD CURVES FOR EH36 AND HY80.

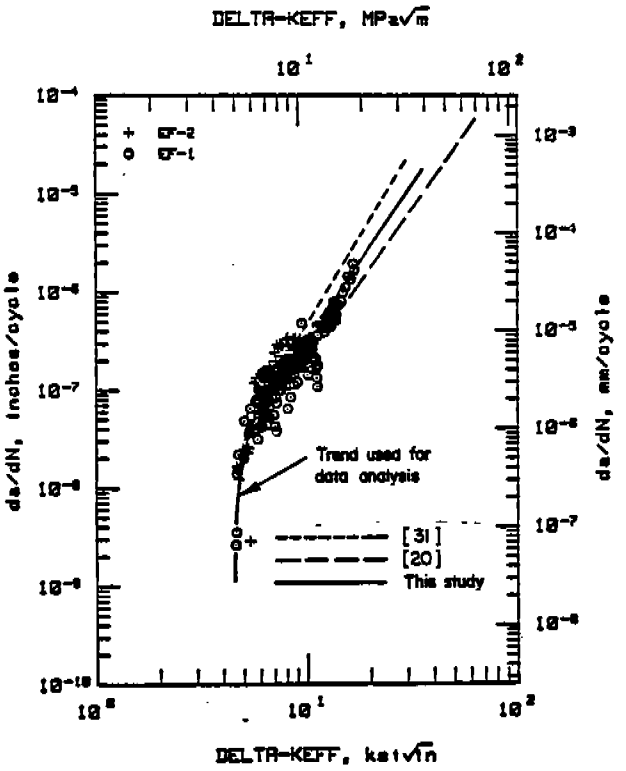

a. EH36 (EF1 and EF2).

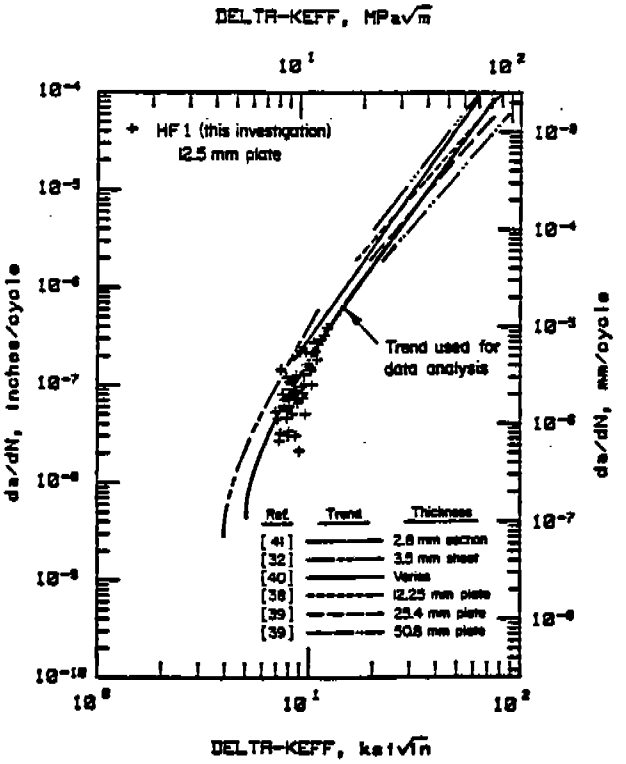

b. HY80 (HF1).

FIGURE 25. CRACK-GROWTH-RATE VERSUS ΔK_{eff} FOR VIRGIN EH36 AND HY80 AT R=0.01 UNDER AMBIENT CONDITIONS.

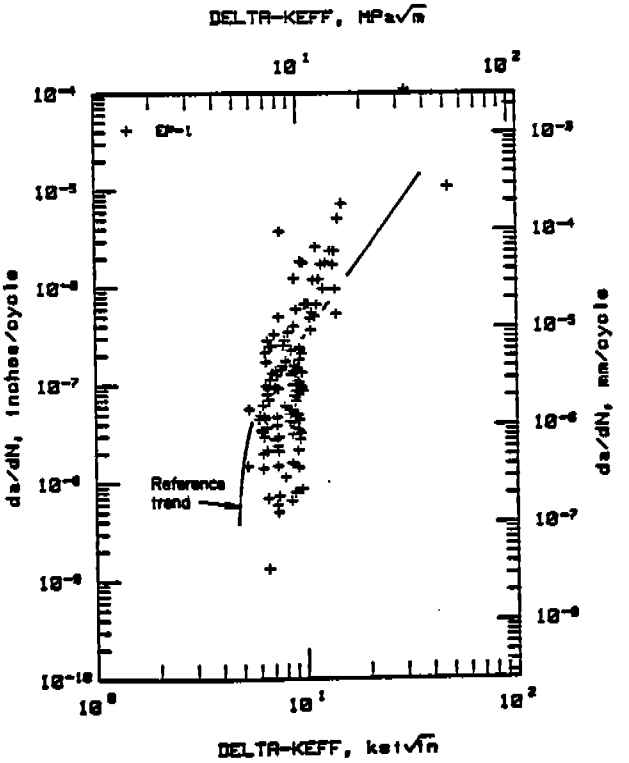

a. EH36 (EP1).

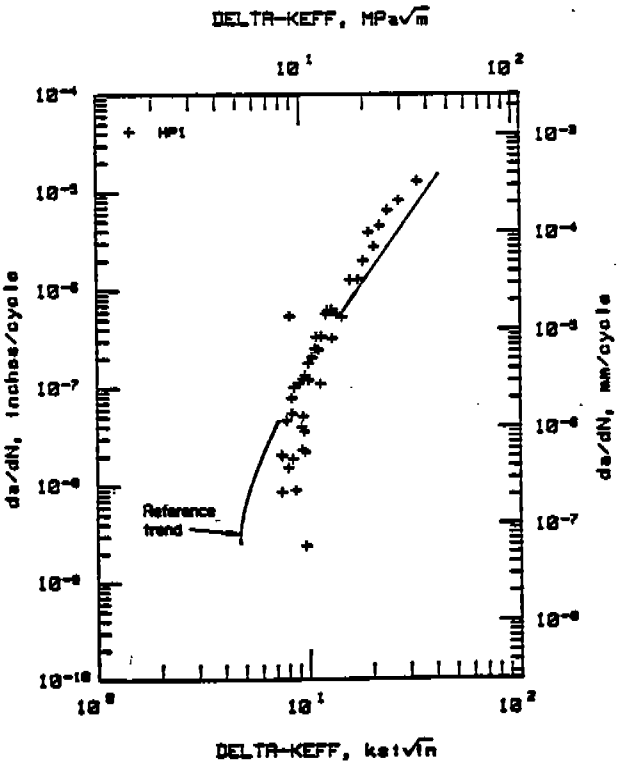

b. HY80 (HP1).

FIGURE 26. CRACK-GROWTH-RATE VERSUS ΔK_{eff} FOR PREDAMAGED EH36 AND HY80 AT R=0.01 UNDER AMBIENT CONDITIONS.

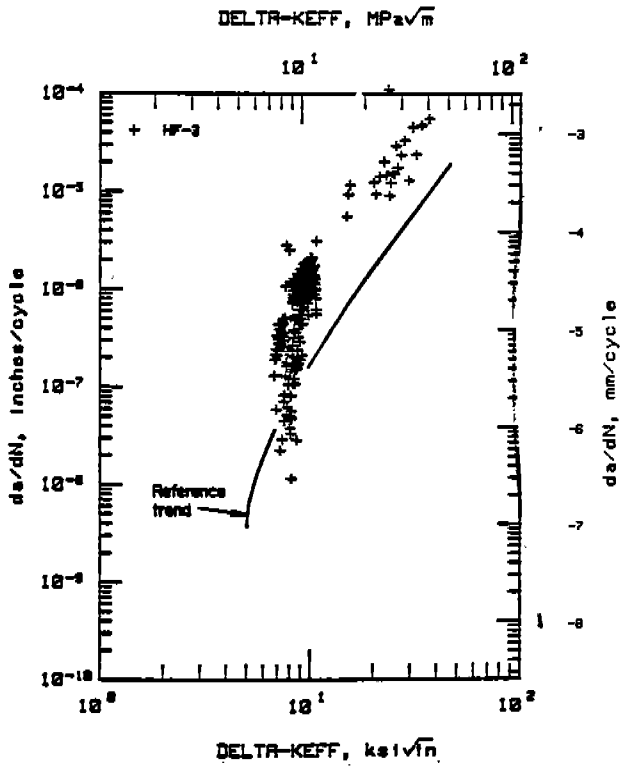

a. Virgin (HF3); f=0.5 Hz.

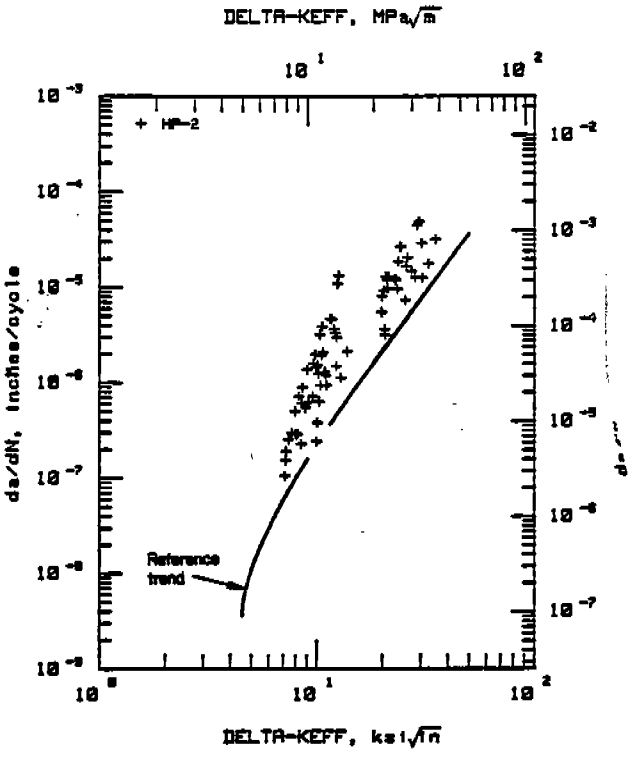

b. Predamaged (HP2); f=0.5 Hz.

FIGURE 28. CRACK-GROWTH-RATE VERSUS ΔK_{eff} FOR HY80 IN SEAWATER AT R=0.01 AND f=0.5 or 0.2 Hz.

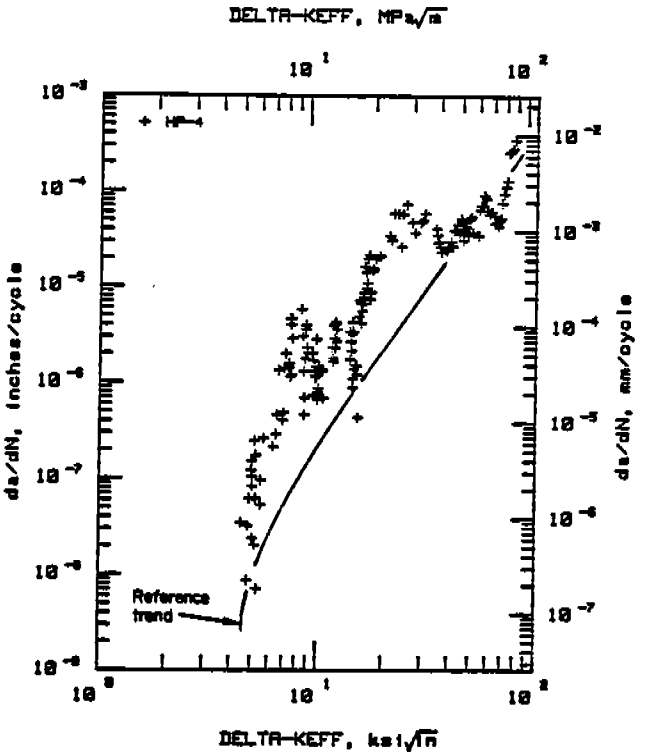

c. Predamaged (HP4); f=0.2 Hz.

FIGURE 28. (Concluded).

COMMITTEE ON MARINE STRUCTURES

Commission on Engineering and Technical Systems

National Academy of Sciences - National Research Council

The COMMITTEE ON MARINE STRUCTURES has technical cognizance over the interagency Ship Structure Committee's research program.

Stanley G. Stiansen (Chairman), Riverhead, NY
Mark Y. Berman, Amoco Production Company, Tulsa, OK
Peter A. Gale, Webb Institute of Naval Architecture, Glen Cove, NY
Rolf D. Glasfeld, General Dynamics Corporation, Groton, CT
William H. Hartt, Florida Atlantic University, Boca Raton, FL
Paul H. Wirsching, University of Arizona, Tucson, AZ
Alexander B. Stavovy, National Research Council, Washington, DC
Michael K. Parmelee, Secretary, Ship Structure Committee, Washington, DC

LOADS WORK GROUP

Paul H. Wirsching (Chairman), University of Arizona, Tucson, AZ
Subrata K. Chakrabarti, Chicago Bridge and Iron Company, Plainfield, IL
Keith D. Hjelmstad, University of Illinois, Urbana, IL
Hsien Yun Jan, Martech Incorporated, Neshanic Station, NJ
Jack Y. K. Lou, Texas A & M University, College Station, TX
Naresh Maniar, M. Rosenblatt & Son, Incorporated, New York, NY
Solomon C. S. Yim, Oregon State University, Corvallis, OR

MATERIALS WORK GROUP

William H. Hartt (Chairman), Florida Atlantic University, Boca Raton, FL
Fereshteh Ebrahimi, University of Florida, Gainesville, FL
Santiago Ibarra, Jr., Amoco Corporation, Naperville, IL
Paul A. Lagace, Massachusetts Institute of Technology, Cambridge, MA
John Landes, University of Tennessee, Knoxville, TN
Mamdouh M. Salama, Conoco Incorporated, Ponca City, OK
James M. Sawhill, Jr., Newport News Shipbuilding, Newport News, VA

SHIP STRUCTURE COMMITTEE PUBLICATIONS

SSC-337 Part 1 - Ship Fracture Mechanisms Investigation by Karl A. Stambaugh and William A. Wood 1987

SSC-337 Part 2 - Ship Fracture Mechanisms - A Non-Expert's Guide for Inspecting and Determining the Causes of Significant Ship Fractures by Karl A. Stambaugh and William A. Wood 1987

SSC-338 Fatigue Prediction Analysis Validation from SL-7 Hatch Corner Strain Data by Jen-Wen Chiou and Yung-Kuang Chen 1985

SSC-339 Ice Loads and Ship Response to Ice - A Second Season by C. Daley, J. W. St. John, R. Brown, J. Meyer, and I. Glen 1990

SSC-340 Ice Forces and Ship Response to Ice - Consolidation Report by C. Daley, J. W. St. John, R. Brown, and I. Glen 1990

SSC-341 Global Ice Forces and Ship Response to Ice by P. Minnick, J. W. St. John, B. Cowper, and M. Edgecomb 1990

SSC-342 Global Ice Forces and Ship Response to Ice - Analysis of Ice Ramming Forces by Yung-Kuang Chen, Alfred L. Tunik, and Albert P-Y Chen 1990

SSC-343 Global Ice Forces and Ship Response to Ice - A Second Season by p. Minnick and J. W. St. John 1990

SSC-346 Fatigue Characterization of Fabricated Ship Details - Phase 2 by K. K. Park and F. V. Lawrence, Jr. 1988

SSC-349 Development of a Generalized Onboard Response Monitoring System (Phase I) by F. W. DeBord, Jr. and B. Hennessy 1987

SSC-350 Ship Vibration Design Guide by Edward F. Noonan 1989

SSC-351 An Introduction to Structural Reliability Theory by Alaa E. Mansour 1990

SSC-355 Relation of Inspection Findings to Fatigue Reliability by M. Shinozuka 1989

SSC-356 Fatigue Performance Under Mulotiaxial Load by Karl A. Stambaugh, Paul R. Van Mater, Jr., and William H. Munse 1990

None Ship Structure Committee Publications - A Special Bibliography 1983